RAPPORT

11 1994

NVE
NORGES VASSDRAGS-
OG ENERGIVERK

Nils-Otto Kitterød

THE HASLEMOEN-PROJECT - MAIN RESULTS AND EXPERIENCES

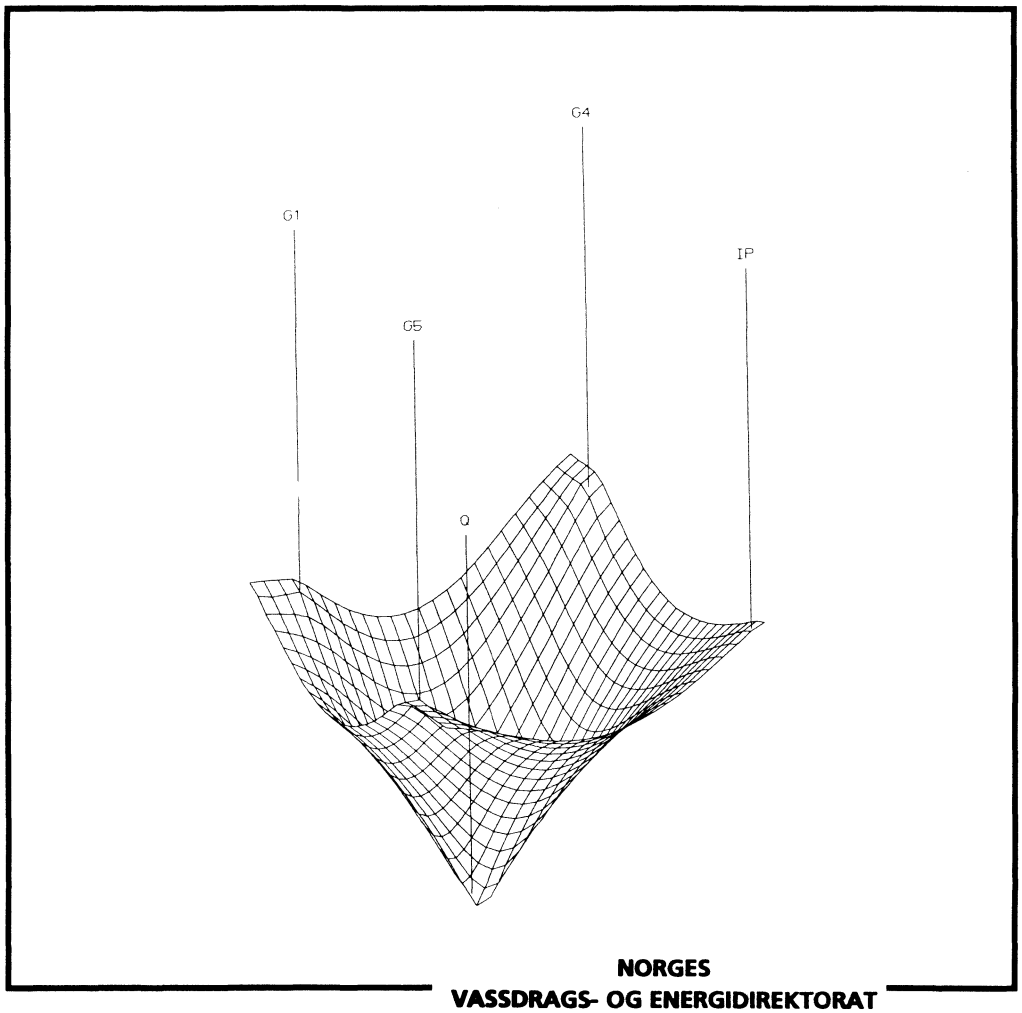

HYDROLOGISK AVDELING

NVE
NORGES VASSDRAGS-
OG ENERGIVERK

TITTEL The Haslemoen-project - main results and experiences	**RAPPORT** 11 - 1994
SAKSBEHANDLER Nils-Otto Kitterød	DATO 17. mars 1994
	RAPPORTEN ER åpen
OPPDRAGSGIVER Norges Teknisk-Naturvitenskapelige Forskningsråd	OPPLAG 25

SAMMENDRAG

Grunnvann kan i enkelte sammenhenger være et konkurransedyktig alternativ til overflatevann som drikkevannskilde. Dette forutsetter imidlertid økte krav til kunnskaper om hydrogeologiske og geokjemiske prosesser i grunnvann og markvann, spesielt hvis det er fare for forurensning av grunnvannsressursene. Dette behovet var bakgrunnen for et tverrinstitusjonelt samarbeide, og Haslemoen ble valgt som et referansefelt for studier av hydrogeologiske prosesser. I prosjektperioden var hovedaktiviteten konsentrert om innsamling av data i felt. Ca. 25 km georadarprofiler ble samlet inn, og en geologisk avsetningsmodell ble utarbeidet. Hydrauliske interaksjoner mellom grunnvann og elvevann er modellert med stor presisjon. Et sporstoff-forsøk i mettet sone ble gjennomført og modellert. Disse delstudiene vil siden danne grunnlaget for videre modellering av forurensningstransport spesielt med tanke på nitratforurensning.

EMNEORD/SUBJECT TERMS
grunnvann
georadar
sporstoff-forsøk
nitratforurening

ANSVARLIG UNDERSKRIFT

Arne Tollan
avd.direktør

Kontoradresse: Middelthunsgate 29
Postadresse: Postboks 5091, Maj.
0301 Oslo 3

Telefon: (02) 95 95 95
Telefax: (02) 95 90 00
Telex: 79397 NVEO N

Bankgiro: 0629.05.75026
Postgiro: 0803 5052055

FORORD

Norge står overfor store utfordringer med hensyn til forvaltning av landets grunnvannsressurser. De to mest aktuelle eksemplene er den nylig inngåtte EØS-avtalen og Stortingets vedtak om utbygging av ny hovedflyplass på Gardermoen. Gjennom EØS-avtalen er Norge forpliktet til å følge EUs krav til drikkevannskvalitet. En håndhevning av disse standardene kan gjøre grunnvann økonomisk interessant for enkelte kommuner. Da Stortinget vedtok å lokalisere Oslos nye hovedflyplass på landets største løsmasseavsetning, ble det satt strenge krav til Luftfartsverket for å sikre grunnvannet mot ekstra forurensning.

Innen forsknings- og forvaltningsmiljøene har man lenge vært oppmerksom på hvilke krav samfunnet vil bli nødt til å stille vedrørende vern og utnyttelse av grunnvann. Samtidig har dette fagområdet lenge vært lavt prioritert. Det var derfor nødvendig med en tverrinstitusjonell satsning for å heve den generelle kompetansen innen dette feltet. Gjennom 'Haslemoen-prosjektet' har fagmiljøene i Oslo regionen gått sammen om å gjennomføre vitenskapelige undersøkelser knyttet til grunnvann.

'Haslemoen-prosjektet' har blitt støttet av Norges Teknisk-Naturvitenskapelige Forskningsråd gjennom programmet "Bedre Bruk av Vannressursene" med til sammen kr 208.000,-. De deltagende institusjoner har bidradd med egenandeler på minimum 50% av feltutgiftene. Kostnader til timelønn for vitenskapelig personell kommer i tillegg. Økte krav til internasjonalt samarbeide har gjort det naturlig for oss å utgi denne rapporten på engelsk.

Av bidragsytere under denne delen av 'Haslemoen-prosjektet' bør nevnes Joseph Allen (Universitetet i Oslo) som har modellert interaksjonen mellom elv og grunnvann, Eyvind Ellingsen (NVE) som har simulert pumpeforsøket numerisk sammen med Nils-Otto Kitterød (NVE), Jens–Olaf Englund (Norges Landbrukshøgskole) som foruten å være en av initiativtagerene til prosjektet også har hatt ansvaret for de kjemiske analysene av grunnvannet og Lars Gottschalk (Universitetet i Oslo) den andre av initiativtagerene, som også har gjort den geostatistiske analysen av grunnvannsobservasjonene. Fannian Kong (Norges Geotekniske Institutt) har deltatt under innsamling av georadardata, og prosessert de tomografiske dataene. Marian Morris (Universitetet i Trondheim) har analysert de geoelektriske resistivitetsdataene. Vibeke Riis (Universitetet i Oslo) har samlet inn og analysert petrofysiske data og utarbeidet en geologisk avsetningsmodell. Jan Steinar Rønning (Norges Geologiske Undersøkelse) har hatt ansvaret for innsamling av georadardata, seismikk og geoelektriske resistivitetsdata. Jarl Øvstedal (Universitetet i Bergen) har bidradd under gjennomføringen av sporstoff-forsøket. Per Aagaard (Universitetet i Oslo) har skrevet den geokjemiske delen av rapporten. Nils-Otto Kitterød har koordinert aktiviteten, simulert forurensningstransporten regionalt og sporstoff-forsøket lokalt.

Oslo, 12. mars 1994

Kjell Repp
seksjonssjef

The Haslemoen-project - Main Results and Experience

In the last few years there has been a growing interest for groundwater in Norway, mainly as a potential resource for water supply. Today Norwegian water supplies rely mainly on surface water, but the contamination level starts to concern the Public Health authorities. Groundwater is to some extent protected from pollution by the unsaturated zone, and is therefore an interesting alternative water supply source. However, pollution may cause serious damage to this resource, and more knowledge is therefor necessary on these issues.

Groundwater and contamination problems are typical interdisciplinary subjects, involving geology, chemistry, hydrology, geostatistics and hydraulics of porous media. This approach requires an inter institutional cooperation. GREGR (Groundwater REsearch GRoup, GREGR 1989) was a direct response to this demand. The first joint project was Haslemoen, and in 1990 GREGR submitted a proposal to the Royal Norwegian Council for Scientific and Industrial Research's (NTNF) R&D programe "Improved Use of the Water Resources" (the BBV Programe) for funding.

1 Introduction

The main purpose of this project was to develop a **reference field** for groundwater research in Norway. The geology of the reference field should not be too complex, and as pollution was a central part of the research, the site should have a well defined contamination history. The Haslemoen aquifer turned out to satisfy most of these criteria and was selected as the study area. The first step was a sedimentological study, and a conceptual model of the geology was developed (chapter 5). The geological model made the framework for a flow model in the saturated zone (chapter 8). The geological mapping was done by using indirect geophysical mapping-techniques (chapter 4), analyses of core- and auger samples and detailed mapping of sand- and gravel pits. A realistic flow model required monitoring of pore flow velocities, and a tracer experiment was necessary. During a 30 days pumping test, we applied 2 tracers that were monitored at 3 pumping tubes. Later we simulated the experiment by a simple analytical model and a more realistic numerical model (chapter 6).

Nitrate contamination of groundwater caused by inorganic fertilizers has been

observed at Haslemoen for some time (Englund et al. 1990). During this project we have supplemented th monitoring equipment, and it is now possible to sample soilwater at different locations and elevations from the nitrate sources to the river bank of Glomma (chapter 9). The nitrate sources are two cultivated fields with mainly wheat, barley and oats.

So far we have described geology and simulated groundwater flow in a deterministic way. An alternative approach that has received much attention in recent research internationally, is stochastic modelling. Some preliminary results from this geostatistic view point are presented in chapter 7. The next step is to apply this stochastic approach in a calibration-validation procedure in a model that includes regional groundwater flow and contamination transport.

This report summarizes only the main results and experience. For further details we refer to articles, reports and theses. (For a summary of field activities supported by the BBV-program, see Table I.)

Table I Main field activities at Haslemoen during the BBV-program period 1990-1992

Field work	Date	Results and aims
Exploration-drilling	May 1990	CPT-analyses and sounding graphs. Valuable geological information.
Core-sampling	May 1990	Sedimentological information. Analyses of petrophysical parameters.
Installation of BAT- equipment	May 1990	To define area of nitrate contamination.
Establish local field at Glomma	May 1990	To study interaction of groundwater and surface water.
Georadar profiling (NGI)	Oct 1990	One good profile obtained. The concept needs some more technical development.
Georadar profiling (NGU)	Apr 1991	Additional geological information from several high quality data profiles.
High resolution seismics and refraction seismics (NGU)	Apr 1991	Good results along the river Glomma.
Preliminary tracer test incl. CP-profiling	Apr 1991	Indication of aquifer parameters. CP-data indicate tracer travel path.
Tracer test	Aug 1991	Monitored drawdown curves and breakthrough curves.
Georadar tomography (NGI)	Apr 1991	To detect tracer and confirm density forced transport and regional flow.
Soil water pressure measurements by BAT-equipment	Sept 1992	Data to be used in a regional flow-model.
Georadar profiling (NGU)	Sept 1992	To try to improve data quality in problem area. To confirm diffuse anomalies above nitrate plume.
Vertical electrical sounding (NGU/NTH)	Sept 1992	Data to be used to correlate electrical anomalies to georadar signals.
Horizontal electrical profiling (NGU/NTH)	Sept 1992	To verify electrical anomaly in nitrate contaminated area.

2 Location

The Haslemoen aquifer located in Våler and Åsnes counties in south east Norway, is approximately 23 km^2 in areal extension and has sediment thicknesses from a couple of meters at Spulsåsen in the north-west to maximum 170 m in the south (Figure 1 and Figure 2). Glomma in south east, the tributary river Hasla to the east, peatbog and shallow deposits in north and west define the boundary conditions of the aquifer. Most of the area is cultivated with potatoes, wheat, oats and barley, the remaining parts are woodlands with mainly pine trees. Large areas of almost horizontal fluvial deposits with terraces at different elevation above Glommas present channel, characterize the geomorphology (Figure 1).

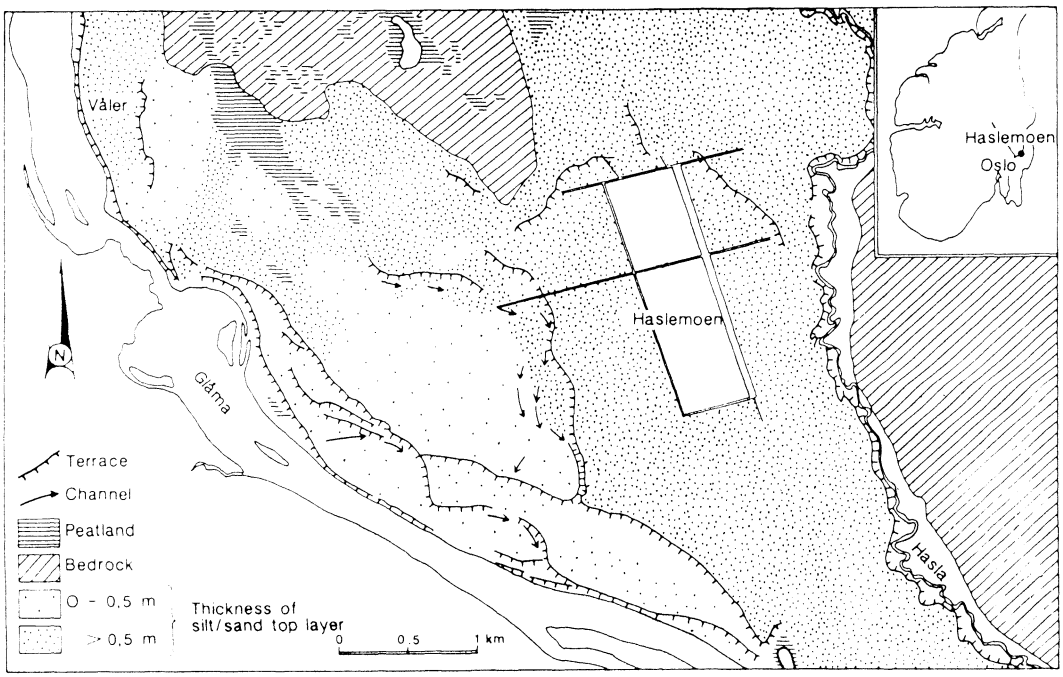

Figure 1 *Key map of Haslemoen showing thickness of top layer ('koppjord'). The white area is cultivated land (Jakobsen et al. 1990)*

The surface soil in the area between Kongsvinger and Våler consists of mainly coarse silt and fine sand, and has a particularly large storage capacity of soil water. This property makes it interesting from a geological, hydrological and especially from an agricultural point of view. The storage capacity and large ability to transport groundwater to the surface by capillary force, minimize the need for irrigation, even when a water deficit occurs during the growth season. This soil has been the subject for several papers (Bjørlykke 1901, Sortdal 1921, Holmsen 1954, Goffeng et al. 1980, 1981a, 1981b). In recent years the attention has been drawn to water budget and recharge studies (Haldorsen et al. 1986, Jakobsen 1987 and Jakobsen et al. 1990) and nitrate leakage to the groundwater

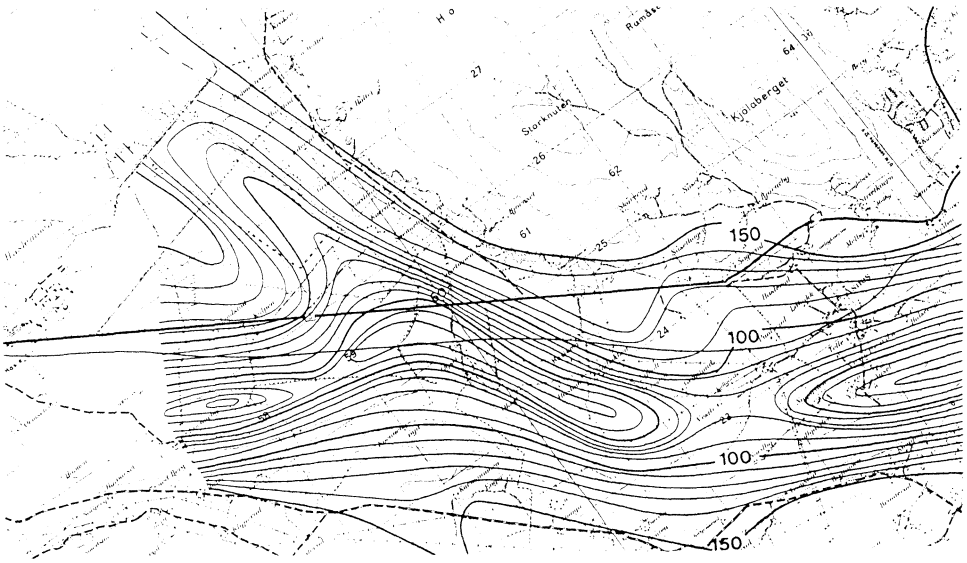

Figure 2 *Bedrock topography mapped by refraction seismics and gravimetry by Høye and Sand, 1983.*

reservoir (Englund and Haldorsen 1986 and Englund et al. 1990).

3 Climate

Meteorological data from Flisa (7 km south-west of Haslemoen) show typical inland climate with cold winters and warm summers. Annual mean precipitation and potential evaporation (calculated by Penmans method) for the period 1961-90 are 617 mm and 365 mm respectively. Approximately 60% of the precipitation falls from May to October, the remaining 40% comes mainly as snow. Potential evaporation corresponds well to growth season and occurs mainly from May to August (Tabell II, DNMI,1991).

Table II Mean Precipitation (R) and Potential Evaporation (PE) from 1931-1960 at Flisa

	May	Jun	Jul	Aug	Sep	Oct	Nov-Apr	Year
R	39	68	87	83	68	57	221	623
PE	78	115	89	62	21	–	–	365

4 Geophysical survey

To get an impression of sedimentary structures at Haslemoen, it was necessary to use indirect mapping techniques. In this project we used two different Ground Penetration Radar (GPR) concepts, an impulse system - Puls Ekko IV (Rønning and Kitterød, 1992), and a multiple frequency radar system (Kong et al. 1990). The Norwegian Geological Survey (NGU) operated the impulse radar equipment and the Norwegian Geotechnical Institute (NGI) the multiple frequency system.

Besides GPR, NGU did conventional high resolution reflection- and refraction-seismics in a few profiles. In september 1992 NGU supplemented the geophysical data with GPR-profiles, vertical electrical resistivity sounding (VES) and horizontal electrical resistivity profiling (HEP). VES and HEP data from the last survey are not yet available.

4.1 GPR, VES and HEP

All together NGU have profiled approx. 25 km with Pulse Ekko IV, 14 km in 1991 and 10 km in 1992 (Figure 3). The multiple frequency radar concept was still under development during this project, and we got only one profile of 1 km length with reasonably good results. Figure 4 illustrates data from one profile sampled by both systems. Both GPR-systems reveals a strong reflector from bedrock at around 25 m depth. Data sampled by Pulse Ekko IV are superior and reveal internal sedimentary structures that are important in order to understand the depositional environment.

Roughly GPR-data from Haslemoen can be grouped in three different classes with respect to data quality (Rønning and Mauring 1991, and Rønning and Kitterød, 1992);

i) areas with good penetration and high resolution
ii) areas with slightly stronger attenuation than in area i)
iii) areas where noise ruins signals

High resolution and good penetration (around 30 m) occur in areas with shallow depth to the groundwater table (2-4 m), open areas at some distance to the wood and generally away from nitrate contaminated areas. The data in Figure 4 represent such an area.

Sampling GPR-data at small paths or close to the wood, usually gave a noisy signal (Figure 5). One possibility that may explain some of the noise, is leakage of energy from antennas to air. Leakage may cause reflections from the wood, and geological significant reflections are difficult (but probably not impossible) to extract. One way to improve signal to noise ratio is to increase the number of traces by decreasing the sampling step (e.g. from 2 to 1 m) and run simple trace averaging in the signal processing. This was a main objective of the 1992 survey.

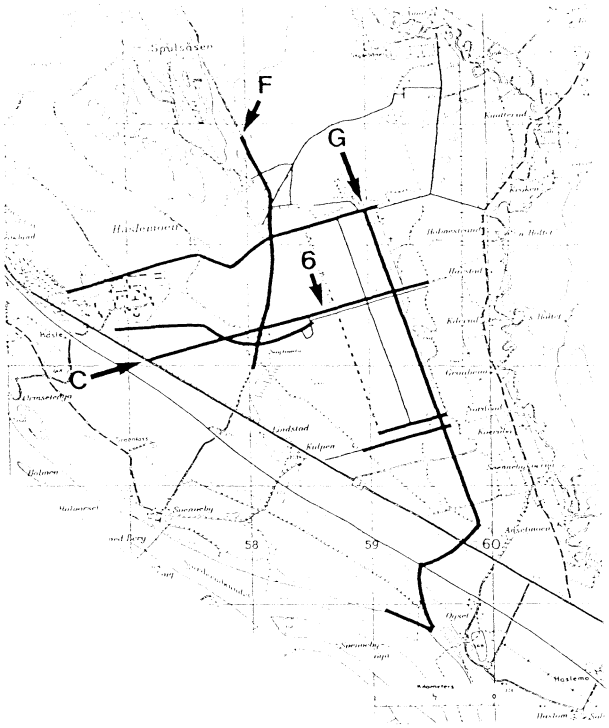

Figure 3 *Sampled GPR-profiles by NGU, in 1991 and 1992.*

An interesting result appears in areas with nitrate contamination. Nitrate in soil water causes an increase in the order of one magnitude in electric conductivity. In the unsaturated zone; 3-4 mS/m in uncontaminated area to 30-35 mS/m in contaminated area. In the saturated zone from 2 mS/m in uncontaminated area to maximum 25 mS/m in contaminated area. High electrical conductivity attenuate electromagnetic waves, and the electrical anomaly from nitrate contamination may shield an underlaying strong reflector. We tried to prove this hypothesis by sampling one profile across the field where nitrate contamination occurs both in unsaturated and saturated zone. Unfortunately wood surrounds the field, and it is not possible to see the shielding without doing further signal processing, which is beyond the scope of this report.

In one of the profiles along the field one strong reflector diminishes gradually downstream (Figure 6). Several causes can explain this. First; the thickness of the unsaturated zone increase from approx. 2 m in the north to approx. 5 m in the south. This will cause an attenuation even without nitrate contamination. (At this point we assume a uniform nitrate concentration in the unsaturated zone). Second; the thickness of the nitrate plume increases downstream because of strong vertical flow components in the saturated zone. Third; because of the underlaying silt unit and a constant nitrate application upstream there may be a slight increase in nitrate contamination in the saturated zone southward. If these two last effects predominates we have an example of attenuation due to a gradually increasing contamination.

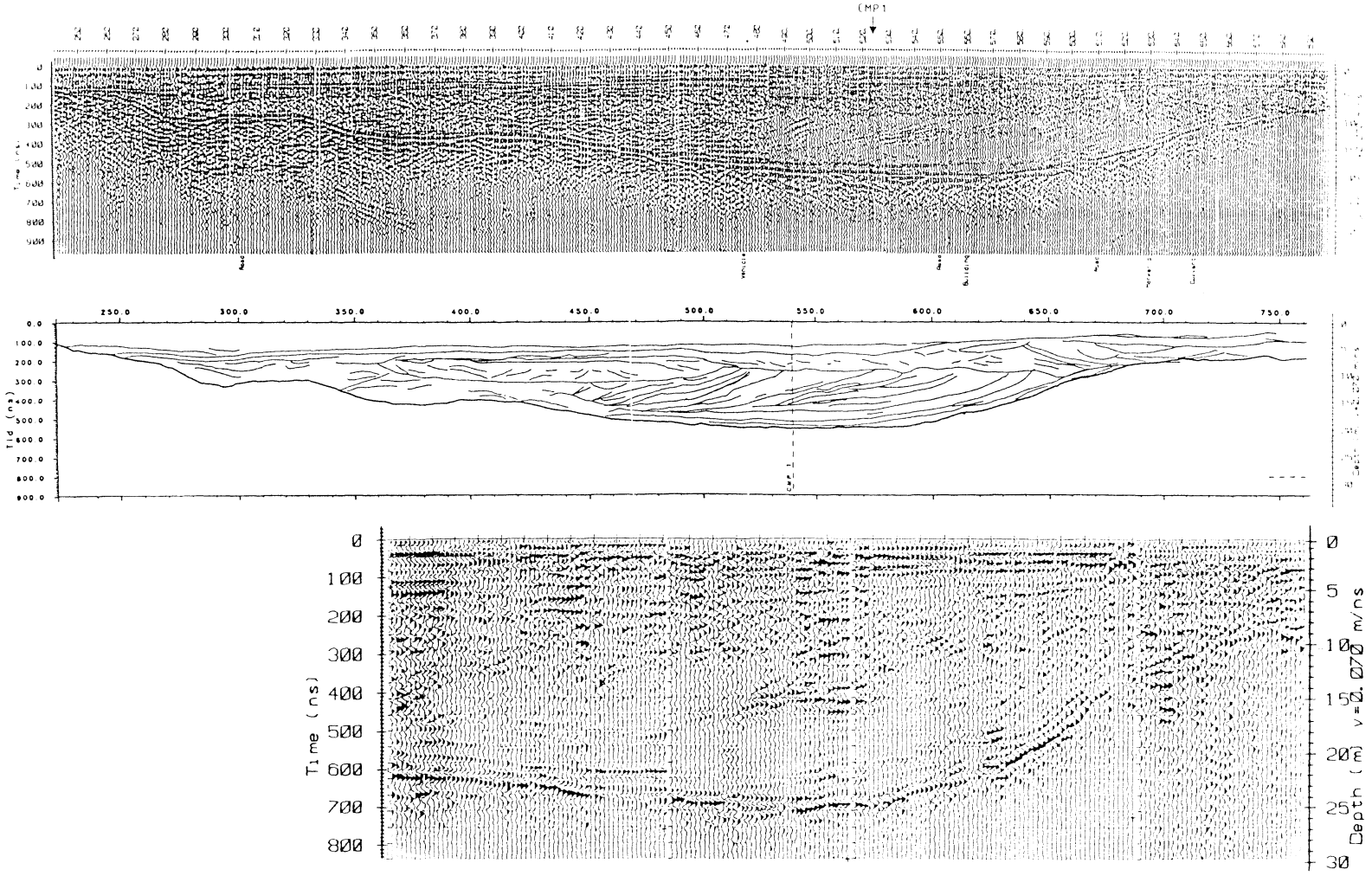

Figure 4. *Ground Penetration Radar data from profile F (Figure 3) sampled by Pulse Ekko IV (upper) and the multi frequency radar concept (lower). The sedimentological interpretation in the middle indicate a channel deposition. Velocity analysis gave average velocity of radar waves in saturated zone of 0.07 m/ns, which correspond to a maximim depth to bedrock of approx. 20 m.*

We made some effort to point out an attenuation of GPR-signals in areas where the contamination occur only in the saturated zone i.e., downstream of the field. In this area the electrical anomaly is at a greater depth and the difference is even more difficult to prove. Besides that, such areas are either entirely in the wood or the depth to groundwater table starts to be a critical factor. This problem will be a topic for further research. To shed more light on this problem we sampled VES and HEP-data.

Detection of a semi horizontal layer appearing in nearly every profile, was a most important result. The depth of this reflector varies from a couple of meters below the surface in the north east close to Hasla south of Åmot, to 15-20 m further south. On top of this persistent reflector there is a unit characterized by unsystematic internal reflections. In some profiles there are reflectors that can be interpreted as channels and channel depositions. The sustained reflector is consistent with the interface to a silt unit discovered from core sampling. The overlaying chaotic unit is well documented through core sampling, auger samples and exploration drilling and consists of layered sand. For further discussion of the results see chapter 5 and Riis (1992). Worth noting are also the consistency in GPR-data and depth to bedrock (Høye and Sand, 1983 and Figure 2.)

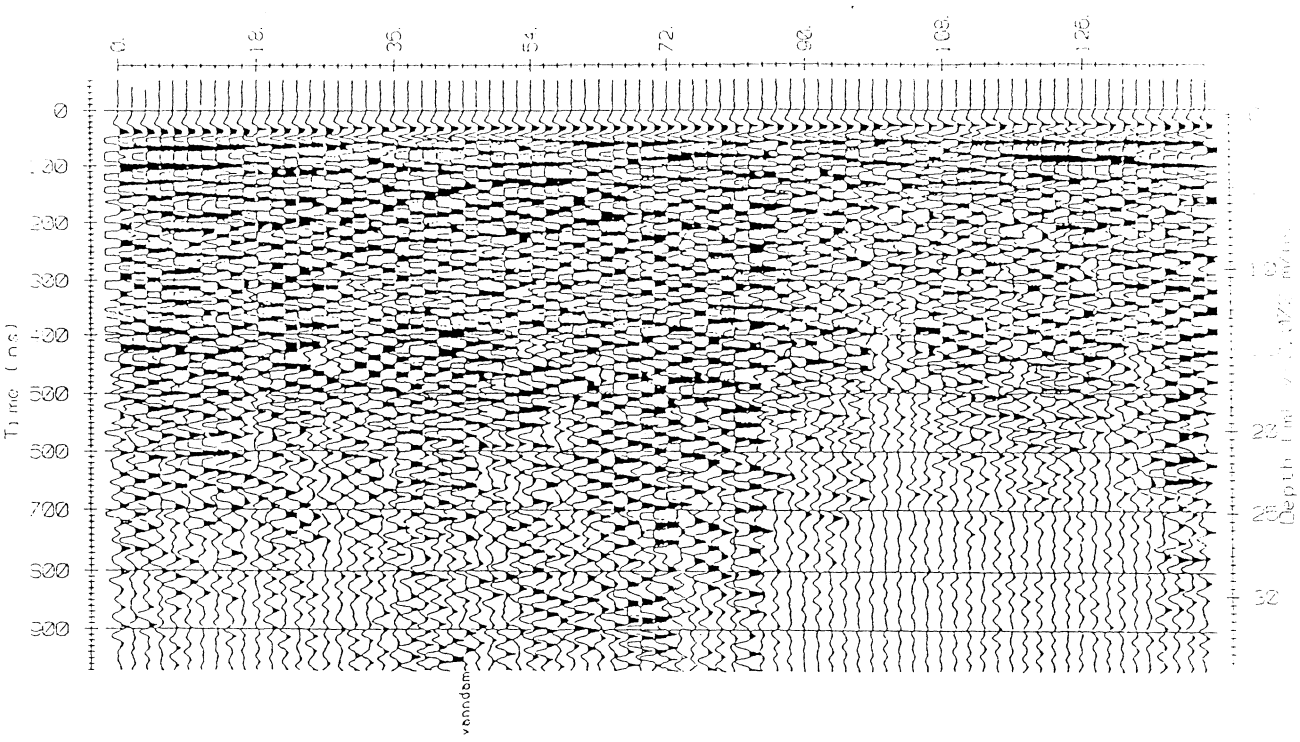

Figure 5 *Example of data sampled in the wood, 6 in Figure 3. The noise is probably due to leakage of energy from transmitter antenna (Rønning and Kitterød, 1992)*

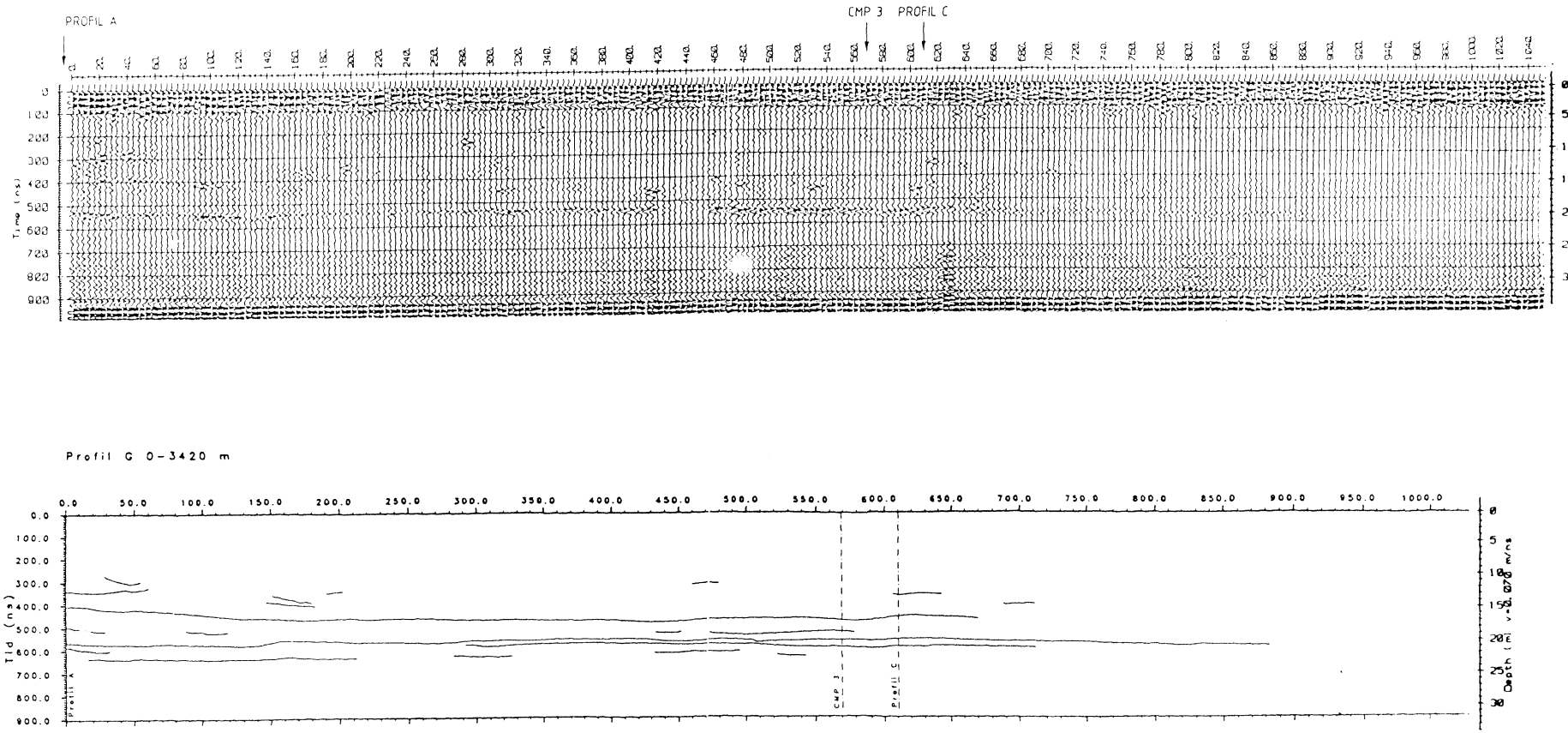

Figure 6 *GPR-data from profile G (Figure 3) illustrating a gradually increasing attenuation of energy from left (i.e. north) to the right.*

4.2 Reflection- and refraction seismics

Seismic surveys on land are time consuming, so only three reflection profiles and one refraction profile was sampled during this project (Figure 3). Sampling followed a so called 'common-depth-point' procedure. By trace-stacking, common-depth-point technique increases the signal to noise ratio, depending on degree of data coverage. In this survey we obtained a 6-fold data coverage. The equipment was a 24-channel digital seismograph (S-2 Echo, Scintrex, Canada), with a center frequency of 50 Hz. Signal generator was a 12-caliber specially designed shotgun.

In the first profile S1 in Figure 3, the bedrock is close to the surface (6-10 m), and reflections from the bedrock and the direct wave (i.e. the shortest traveltime from source to receiver) occur almost at the same time. This makes it difficult to distinguish between the reflections and the 'tail' of the direct wave. This reflection technique is therefore not suitable for detecting targets at less than 15-20 m depth. Refractions on the other hand, can be identified in this profile, and suggest a depth to bedrock of approx. 9 m at the beginning of the profile.

At profile S2 the depth to bedrock was approx. 25 m. In this area another problem arose, namely loose packed unelastic surface soil (cfr. 'koppjord'). Unelastic matter cause strong attenuation of the high frequency energy. In addition this surface soil provide poor acoustic contact from energy source to soil and from soil to receiver. Of those reasons bedrock reflections in this area, was hard to detect.

At profile S3 at the Glomma river bank (Figure 3), water saturates the soil almost to the surface. This condition caused a good acoustic contact between soil and energy source, and the depth to bedrock was large enough to distinguish between multiples and reflections. Profile S3 rendered the most valuable experience with reflection seismics at Haslemoen. NGU determined the depth to bedrock to 80 m with at least 5 strong internal reflectors. To improve velocity analysis we did a seismic refraction profile that gave average soil velocities of 1500 m/s.

5 Geology

A realistic groundwater flow model is based on the knowledge of aquifer geometry and a basic understanding of the geological characteristics. Høye and Sand (1983) estimated depth to bedrock by gravimetry and seismic refraction (Figure 2) and proposed a sedimentological model of the aquifer, but the internal structure and hydraulic properties of the aquifer were still uncertain. On this background it was

necessary to make an effort to establish a more precise sedimentological model of the aquifer.

Retreat of the Late Weichselian icecap in eastern Norway, draining of glacierdammed lakes, fluctuating sea levels and isostatic land elevation controlled the sedimentation of the main sedimentological units at Haslemoen. On the basis of drilling, core sampling and geophysical mapping, the sediments of Haslemoen can be classified in six stratigraphical units (Figure 7). To some extent the environment of deposition can be specified.

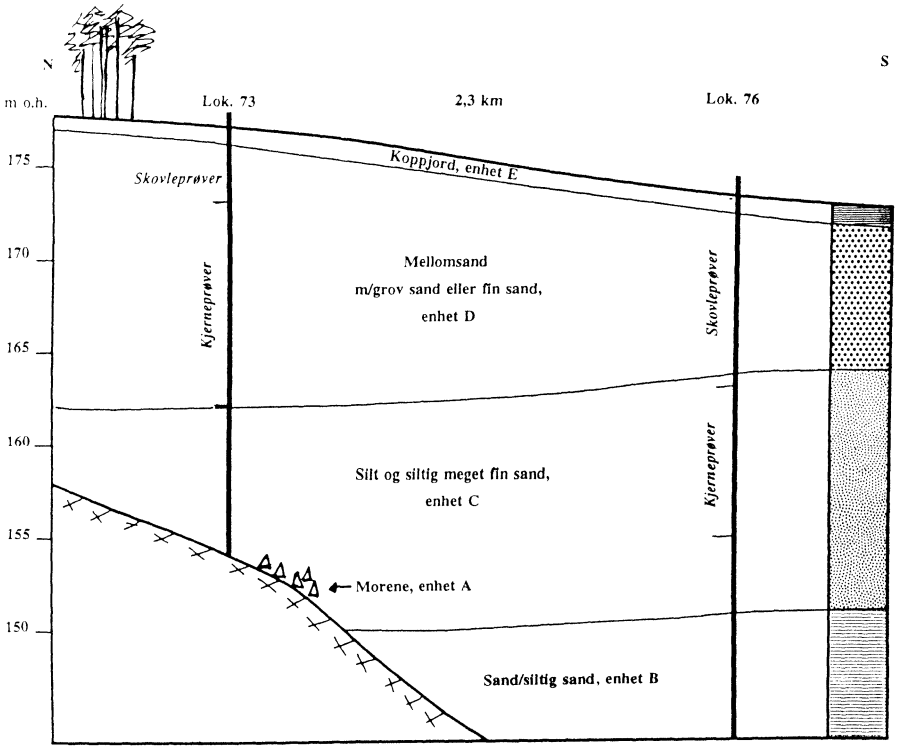

Figure 7 *Illustration of Facies at Haslemoen. **A**-till, **B**-sandy silt, **C**-silt-fine sand, **D**-layered medium sand, **E**-silt ('koppjord') Riis, 1992.*

Above bedrock there is a discontinuous till of 2-3 m thickness (unit A). A glacier near brackish-marine unit (B) is overlaying bedrock and till up to 150 m a.m.s.l. This unit, which is poorly mapped, was probably deposited from 9500 to 9200 BP (BP - before present) when the icecap retreated from Haslemoen to Elverum. Unit C is fluvial silt of 12-13 m thickness and overlays unit B in the whole area from approximately 150-164 m a.m.s.l. This unit is probably connected to the catastrophic draining of the glacierdammed lake 'Nedre Glåmsjø' 9200 years BP. A meandering river system eroded the silt unit, and deposited point bars from 157-174 m a.m.s.l. (unit D'). During a new period with increasing river discharge the

fluvial medium sand unit (D) was deposited. Unit D that has a chaotic signature in the GPR-profiles, similar to what we expect from a braided river system. This unit are deposited all over the valley from 150-180 m a.m.s.l. and consists mainly of fluvial medium sand. The surface sediment unit E is silt ('Koppjord'), probably an overbank deposit. The isostatic land elevation caused a lowering of the erosion basis. Glomma eroded the sediment and caused the characteristic terraces surrounding the river today (Riis, 1992).

6 Porewater flow velocity

Calibration of groundwater models is usually done with respect to hydraulic head. Hydraulic head is not very sensitive to inhomogeneities in the aquifer. Pore flow velocities on the other hand, is very sensitive to aquifer inhomogeneities. The crucial question when dealing with chemical contamination is pore velocities or residence time in the aquifer. Accordingly a main purpose of the field activity in this project was to monitor porewater flow velocities. This is an essential part in groundwater modelling when chemical contamination is the ultimate problem.

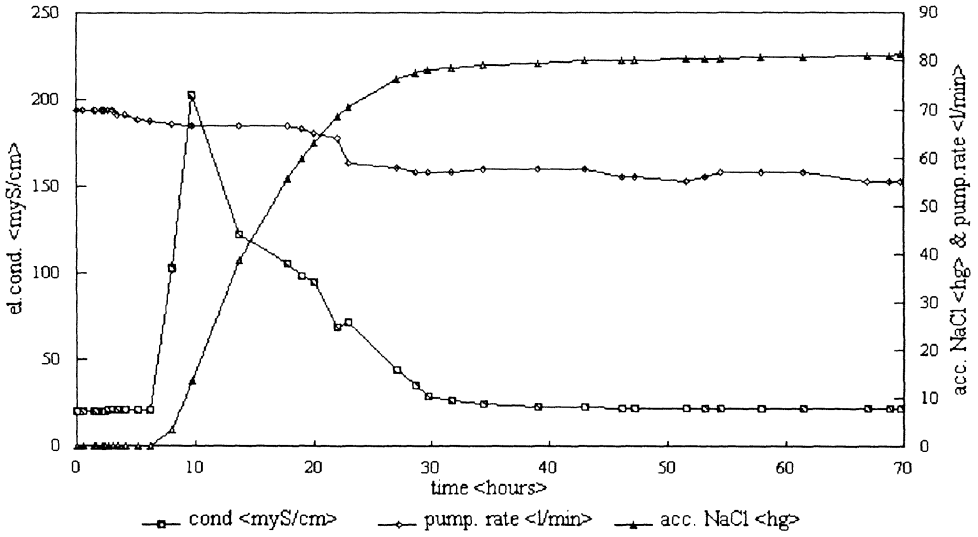

Figure 8. *Preliminary tracer test (loc.8 in Figure 9). Break-through occured after 8 hours. Of 14 kg Total Dissolved Solid was 8 kg recovered.*

Our main concern was the average pore velocity on a macro scale. Average pore velocities can be monitored indirectly by imposing a tracer into the aquifer. As the gradient of the hydraulic head is a driving force to flow, a main decision is whether the velocity should be monitored with the naturally gradient or with an imposed gradient in addition to the regional flow gradient. Natural pore velocities

may be in the order of a few centimeters to several meters per day in the Haslemoen aquifer, and we considered this uncertainty to be so large that we decided to impose a gradient to speed up the velocity. This approach assumes that pressure is monitored in detail.

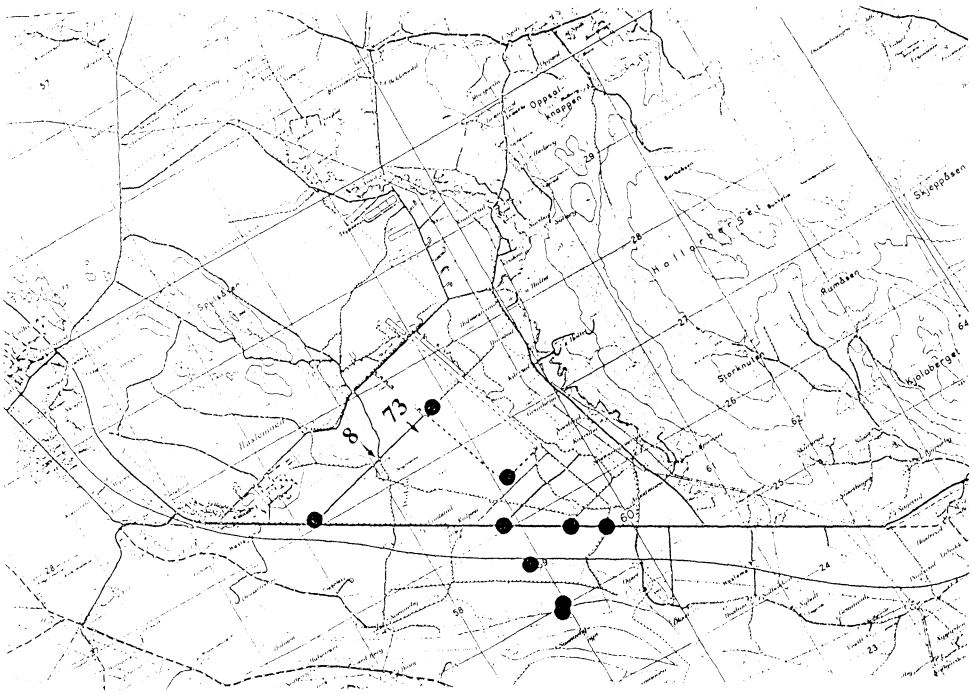

Figure 9. *Tracer test was performed at location 73, and preliminary tracer test at loc. 8. Markers indicate location of BAT-equipment*

Preliminary tracer test with CP-monitoring

To gain some experience a preliminary tracer test with salt (NaCl) was performed in 1991 (500 m to the west of the subsequent tracer test). In this preliminary test, previous installed tubes and piezometers were utilized and the direction between injection- and pumping tube was normal to the regional groundwater flow. Pumping rate started at 5.4 m^3/h and fell gradually off to 3.3 m^3/s (due to shrinkage in a plastic pumping tube). Distance between injection and pumping tube was 3 m. Manually collected water samples were taken, and the NaCl concentration determined indirectly by measuring the electrical conductivity.

Breakthrough occurred after 7 hours and maximum concentration passed after approx. 10 hours with 10 times the initial el.conductivity. After approx.50 hours of pumping the el.conductivity had decreased almost to the initial conductivity (6% higher than initial condition, Figure 8). NGU performed a Charged Potential

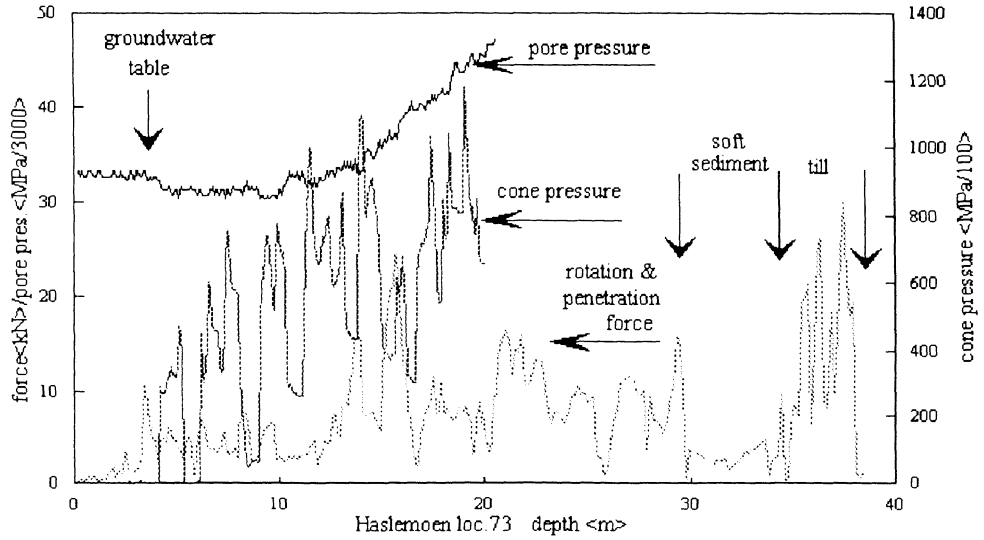

Figure 10. *Results from exploration drilling at loc. 73 (Figure 9), indicating silt at top, layered sand to 29 m below surface,and till above bedrock.*

(CP) monitoring of this test, and was able to detect an electrical anomaly corresponding to the salt pulse moving from injection to pumping tube (Morris et al., 1992). From this monitoring pore flow velocity and flow direction was possilble to define. Probably a minor part of the salt escaped from pumping because of the regional flow perpendicular to the injection-pumping direction. Indication of the amount of tracer escape is also possible to interpret from this data. Unfortunately it was not possible to carry out CP-monitoring during the later tracer test. However, if tracer tests in the saturated zone should be performed in the future with or without pumping, CP-monitoring is recommended.

Local geology

The tracer test was performed 200 m to the west of the corn field at point 73 (Figure 9). Geological details were available through exploration drilling and pressure test (CPT) performed by NGI (Figure 10). From core samples 4-13 m below surface, Riis (1992) analyzed hydraulic conductivity, porosity and grain size distribution (Figure 11).

The main result from this analysis is the following geological model; above bedrock at 38 m below surface, there is a 4 m till deposition. A coarse silt-fine sand unit of approx. 4 m thickness is overlaying the till. From approx. 30 m to 1.5 m below surface there is a stratified sand unit with medium to fine sand. Groundwater table is 4 m below surface. The top soil is coarse silt ('koppjord').

For Norwegian conditions this stratified sand unit is remarkably homogeneous. Variance of hydraulic conductivity is larger with respect to estimation techniques

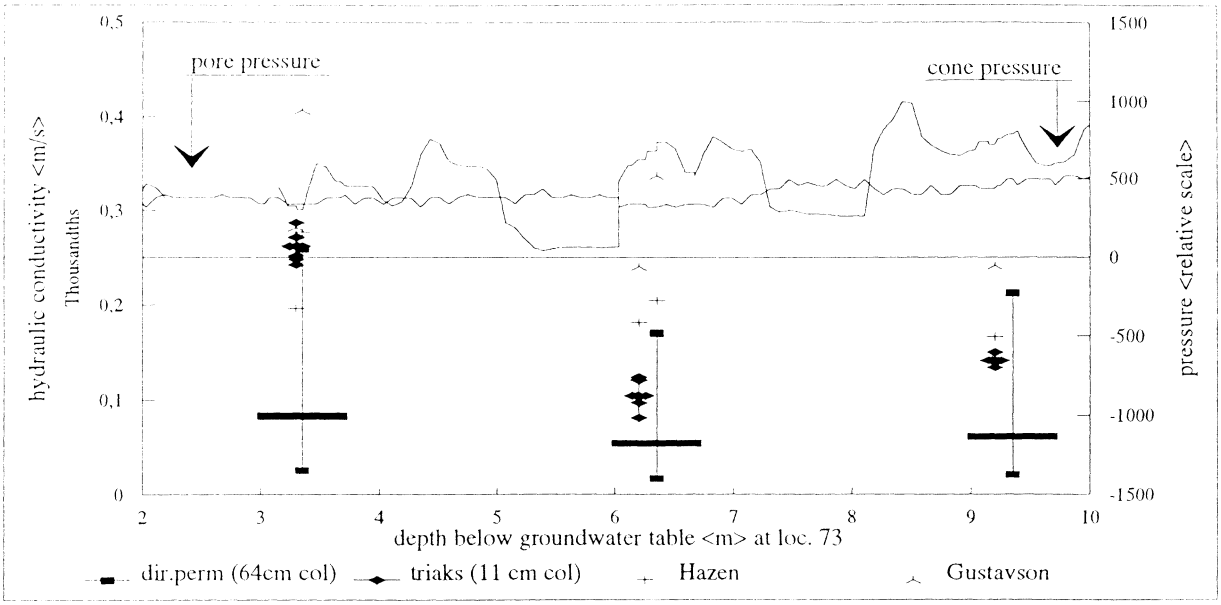

Figure 11. *CPTU curve (Figure 10) and estimates of k (Riis, 1992). Vertical line for dir. perm indicate uncertainity in estimate.*

Variance of hydraulic conductivity is larger with respect to estimation techniques than actually variance of estimates from samples to samples (Figure 11). Direct permeability measured from whole core samples of 64 cm length, varies from (6.1-8.3)· 10^{-5}m/s, while Hazen's and Gustafson's estimates from grain size distribution give values from (1.7-2.0)· 10^{-4}m/s and (2.4-2.8)· 10^{-4}m/s respectively. From triaxial tests with cores of 11 cm length, the mean value varies from (1.0-2.6)· 10^{-4}m/s,

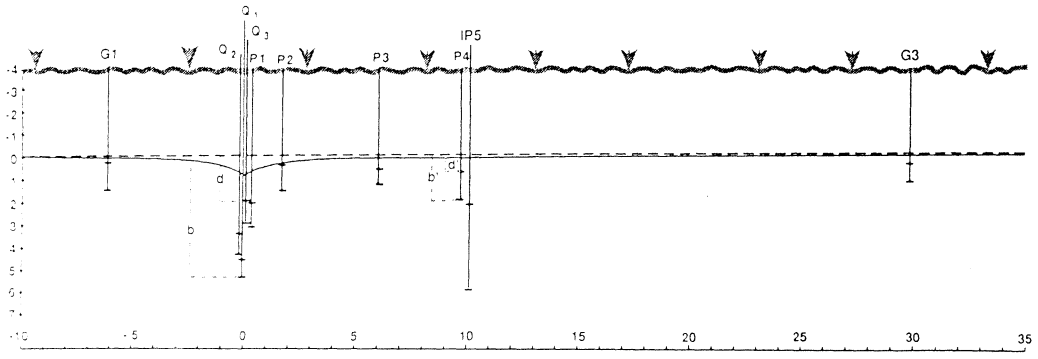

Figure 12. *Pumping- (Q), monitoring- (P and G) and injection tubes (IP). The dashed line indicate groundwater table before pumping, and the solid line maximum drawdown.*

with only a minor decrease in permeability as a function of increasing pressure. These results indicates that compressibility of the sediment can be neglected in this part of the aquifer. There is however a trend in the estimates that indicate a slightly decreasing hydraulic conductivity with increasing depth. Porosity is estimated to be around 25%. For further details see Riis (1992).

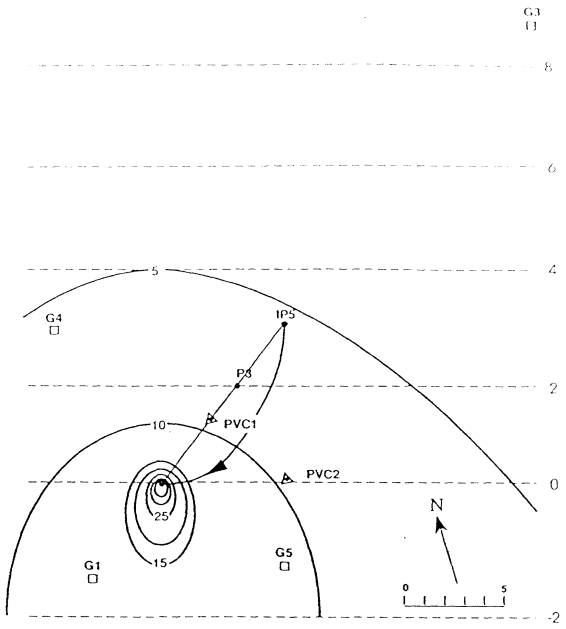

Figure 13. *Set-up of the experiment in horizontal plane. The dashed line indicate groundwater table before pumping, contour interval in cm.*

Set-up of experiment

The stratified sand unit is approx. 25 m thick below the groundwater table. Of economical reasons we did not screen the whole aquifer, either in sections nor with one well. 3 pumping tubes, 32 mm in diameter and with 70 cm long filtertips at 2-5 m below the groundwater table, penetrated 12 % of the aquifer. The injection tube had a 4 m long screen and was located 10 m away from the pumping wells. The injection screen covered the same depth interval as the pumping filters. Drawdown was monitored automatically in 4 piezometers and manually in 6 tubes (Figure 12, Figure 13 and Figure 14). Pumping rates was 1.8 m^3/h for the upper tube (2.0-2.7 m below initial groundwater surface), 1.65 m^3/h for the intermediate tube (3.4 - 4.1 m depth) and 1.6 m^3/h for the deepest tube (4.4 - 5.1 m depth). These pumping rates were constant during the whole pumping period, only interrupted by maintenance of the power generator or by technical problems. The pumping period was 30 days and a steady state flow condition was not fully achieved (Figure 15).

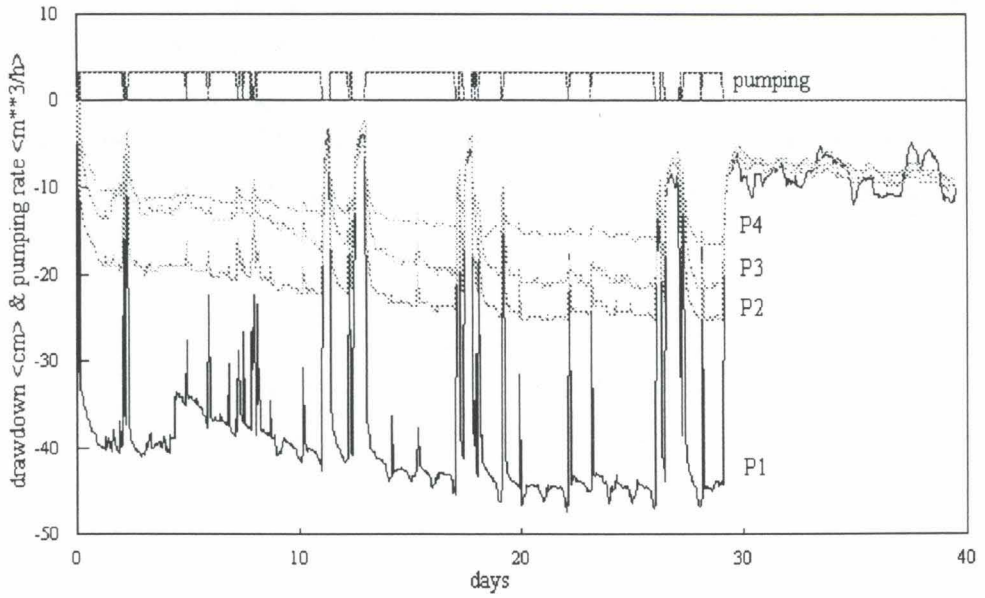

Figure 14. *Drawdown monitoring form 12.08.-20.09.91 at loc.73 (Figure 9). The irregular character in drawdown is due to pumping breaks.*

We used two different tracers, Rhodamine-WT and NaCl. We recharged 43.43 g dissolved Rhodamine and 35 kg salt dissolved in 300 l water into the injection tube after approx. 5 hours of pumping. At the pumping tubes we sampled electrical conductivity every 2nd minute. Water samples were taken to detect Rhodamine (detection limit 0.2 ppb). One of the electrical conductivity sensors probably broke down before we detected any electrical anomaly (Q3 in Figure 17). The electrical anomaly occurred earlier than break-through of Rhodamine both at Q1 and Q2 (Figure 18).

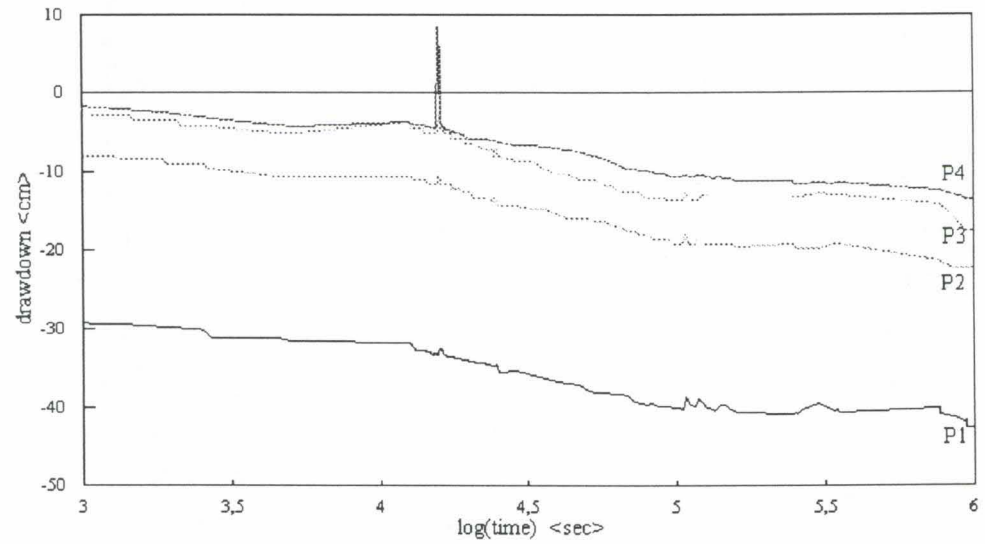

Figure 15. *Drawdown corrected for irregularities (Figure 14). Note the spike that shows the response in the aquifer to injection of 300 l tracer.*

We recovered only 2.3 g Rhodamine-WT i.e. 5.3 % of injected tracer. Obviously there have been a large escape of tracer from the pumping tubes, and some fraction have most likely been adsorbed in the sediment matrix. The amount of adsorbed matter have not yet been quantified.

The recovery of salt is more complicated. After the first recession in salt concentration, the concentration started to increase in Q1 and did not cease during the pumping period (Figure 17). This can be explained by the great salt concentration (approx. 10 %), that have a rather large density contrast to fresh water. The salt could therefore sink downwards before it was recovered. Gravity is very important in this tracer test because of the slow pore flow velocities around the injection tube. Another possibility to the increase in salt concentration at the

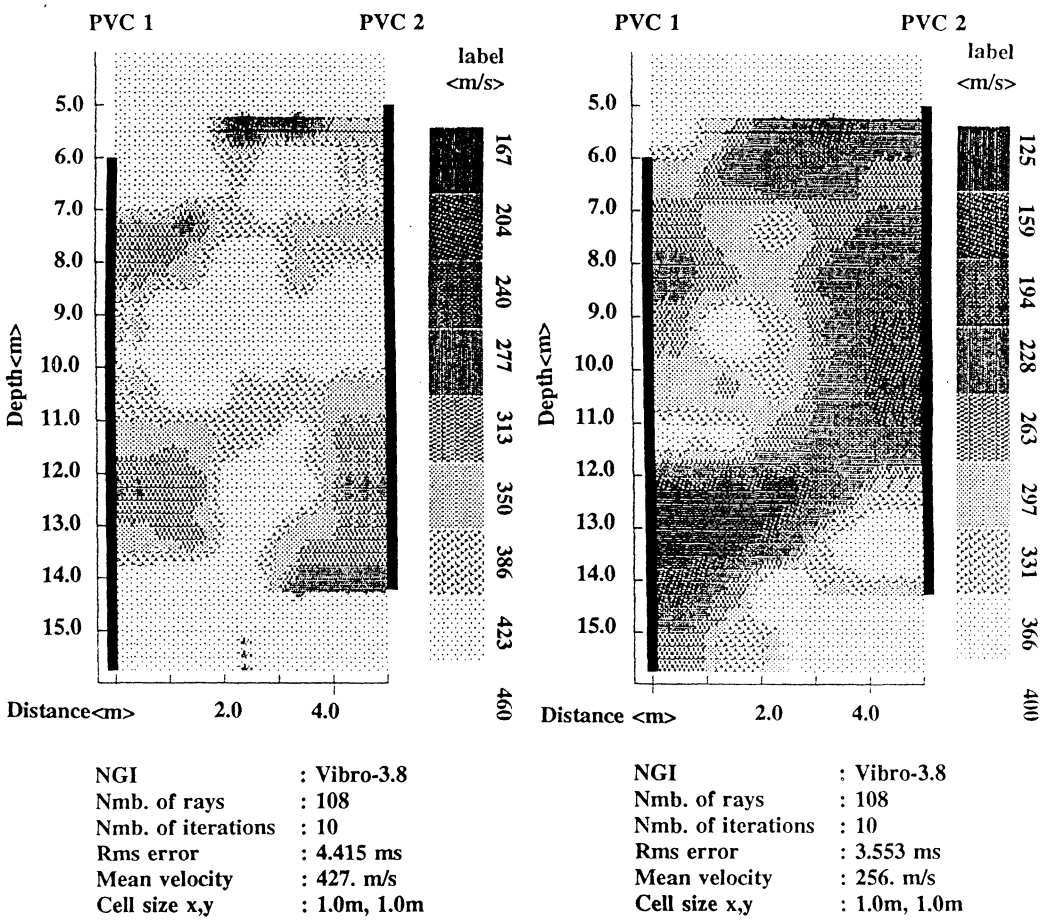

Figure 16. *Radar tomography between PVC 1 and PVC 2 (Figure 13). Left before injection, right after break-through of NaCl. (Attenuation=1000 dB/velocity).*

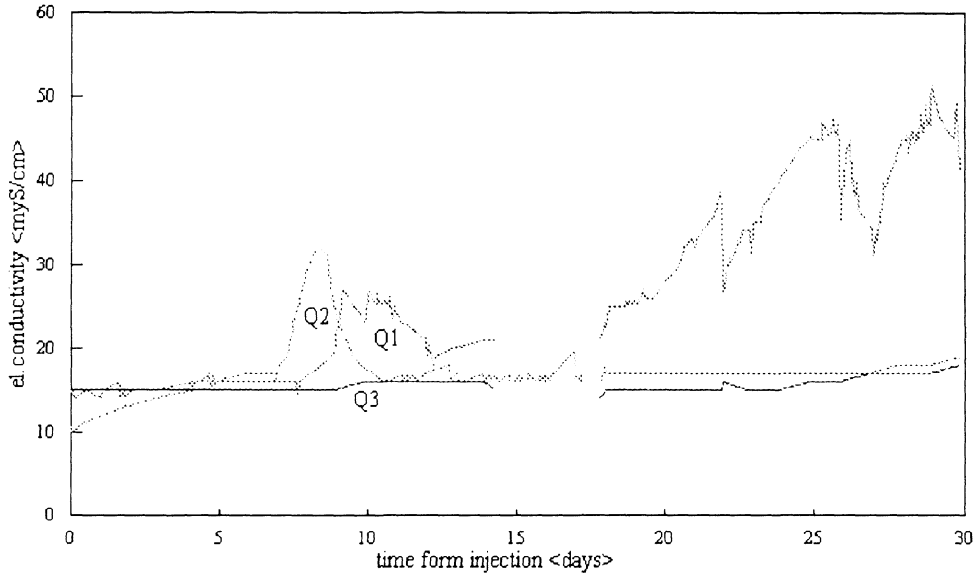

Figure 17. *El.conductivity corresponding to NaCl concentration. Note increase in NaCl concentration at the end of pumping in the lowest pumping tube, Q1.*

end of the pumping period, is that all the salt crystals may not have been dissolved before injection. This crystals would then sink to the bottom of the injection tube and gradually dissolve.

Accordingly the escape of salt have most likely been greater than for Rhodamine-WT. Escape of salt is confirmed by an electromagnetic tomography performed by

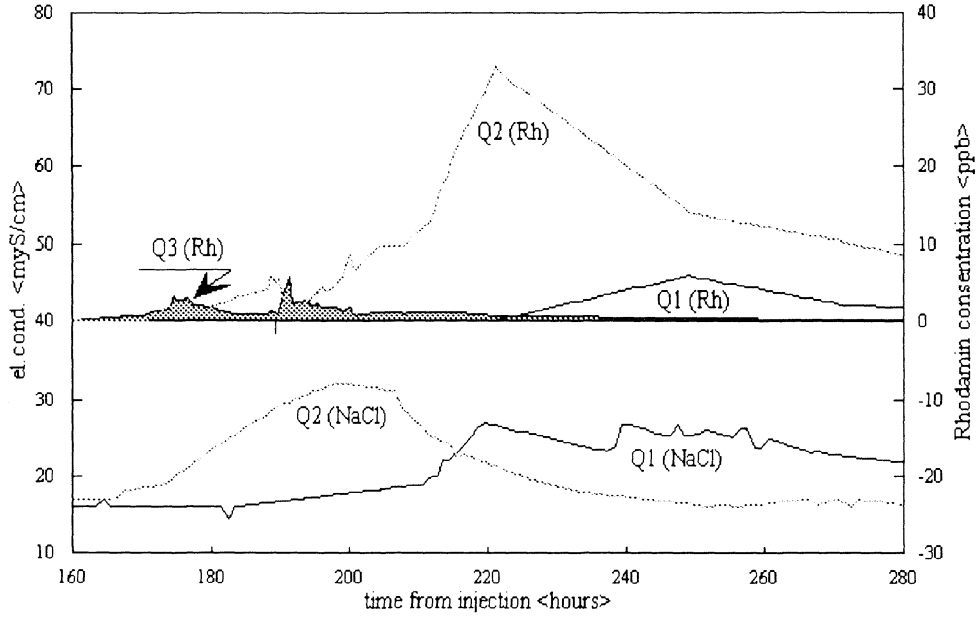

Figure 18. *Break-through of Rhodamine and NaCl. Increase of Rh. concentration in Q3 at vertical bar was due to 1 hour pumping break at Q1 and Q2 while Q3 pumped.*

NGI at to PVC-tubes during the tracer test. One of this tubes was located right downstream to the injection tube with respect to the regional flow direction (PVC2 in Figure 13). The other PVC tube was located between the injection an the pumping tube. The attenuation of energy was greatest in the PVC-tube downstream of the injection tube (Figure 16).

Regional flow

To minimize the escape of tracer the direction between injection and pumping should be parallel with respect to regional groundwater flow. As indicated in the groundwater table map there is a minor anomaly in the groundwater flow in the tracer test area (Figure 19). The regional flow direction is therefore somewhat difficult to monitor. Pumping and injection tubes were installed before the local flow direction was determined in detail. Accordingly, injection-pumping direction was 30° off the regional flow direction.

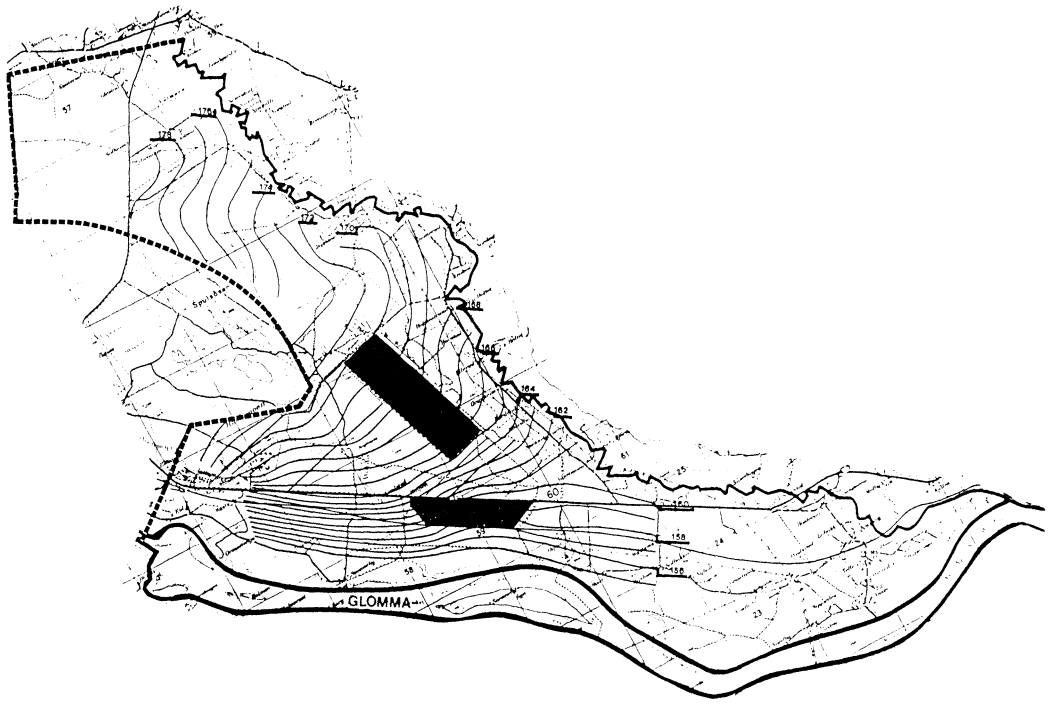

Figure 19. *Groundwater table mapped by Englund et al. in june 1985.*

The gradient of the groundwater table in the flow direction is of the magnitude $2 \cdot 10^{-3}$. The drawdown of the water table around the pumping tube is not entirely concentric circles, but is elongated in the regional flow direction (Figure 13). However, the gradient between injection and pumping tube increased an order of magnitude; to $1.4 \cdot 10^{-2}$ (G3-P1) and $7.0 \cdot 10^{-3}$ (G3-P2). So as a first approximation the regional groundwater flow may be neglected.

6.1 Analytical simulation of drawdown and break-through curves

The main purpose of this tracer test was to monitor pore flow velocities. Pore flow velocities are a function of hydraulic conductivities, porosities and gradients of hydraulic head, $\nabla\phi$. With a relatively homogeneous aquifer, good estimates of petrophysical parameters and well monitored drawdown and break-through curves, pore flow velocities should be possible to model.

The first step was to simulate drawdown and break-through curves with an analytical solution based on assumptions of a simplified geological model. This simple analytical solution is well suited to analyze sensitivity in drawdown and break-through with respect to different petrophysical parameters. The next step was to calibrate a numerical model under the same conditions as the analytical model, primarily to gain some numerical experience with the code and to make proper decisions with respect to boundary conditions and how to discretize the flow field. The final step not yet achieved, is to apply a more realistic model of the geology in the numerical model.

Analytical approximation

The response of water abstraction from a well is usually analyzed by applying the observed data to type curves developed from analytical solutions that represent different simplifying approximations of the true flow. Several analytical methods are discussed by Kruseman and de Ridder, 1992. In resent years analytical solutions are developed to handle aquifers with more realistic geology (Wikramaratna 1984, Maas 1987, Székely 1992), and it seems to be a need for analytical simulations as an alternative to rigorous numerical simulations (Veling, 1991).

At local scale around point 73 the Haslemoen aquifer can with some reservations, be considered homogeneous, but with a distinct stratification. At first we assumed that the aquifer was isotropic. Later we changed this assumption and considered the aquifer to be anisotropic with respect to the horizontal and vertical flow directions.

Maximum drawdown was approx. 40 cm and the thickness of the aquifer is minimum 25 m. The gradient in the flow direction $\boldsymbol{dh/dr}$, had a maximum of 0.02 between P2 and P3. As $\boldsymbol{dh/dr \ll 1}$, the flow is mainly horizontal (Dupuit-Forchheimer assumption, Bear and Verruijt 1987), and the equations for a confined aquifer may be applied. (This assumption is somewhat violated for $\boldsymbol{r < 1.8\ m}$ i.e. for P1 and P2.)

If we neglect the regional groundwater flow gradient, which is of the order $dh/ds \approx 1 \cdot 10^{-3}$, the radial flow equation in a homogeneous isotropic confined aquifer is described by the differential equation (Bear, 1979);

$$\frac{\partial^2 s}{\partial r^2} + \frac{1}{r}\frac{\partial s}{\partial r} + \frac{\partial^2 s}{\partial z^2} = \frac{S}{T}\frac{\partial s}{\partial t} \qquad (1.1)$$

where s is the drawdown at a time t at a radius r and depth z, $s(r,z,t)=\phi_0 - \phi(r,z,t)$. S and T is the storativity and the transmissivity of the aquifer respectively.

The initial and the boundary conditions are (b and d explained in Figure 12):

$$s(r,z,0) = 0 , \qquad s(\infty,z,t) = 0 ,$$

$$\frac{\partial s(r,0,t)}{\partial z} = 0 , \qquad \frac{\partial s(r,D,t)}{\partial z} = 0$$

and

$$\lim_{r\to 0}(b-d)r\frac{\partial s}{\partial r} = \begin{cases} 0 & for \quad 0<z<d \\ -\dfrac{Q_w}{2\pi k} & for \quad d<z<(b-d) \\ 0 & for \quad z>b \end{cases}$$

Where Q_w is pumping rate, k is hydraulic conductivity and D is aquifer thickness. In the following transmissivity T is replaced by kD.

According to Hantush (1961) the solution can be divided in to two parts $W(u)$ and f. $W(u)$ is the Theis-well function which takes the horizontal flow component into account, while f is the additional drawdown due to a partially penetrating well. This latter flow component is both vertical and horizontal. From Hantush (1961) we get;

$$s(r,z,t) = \frac{Q_w}{4\pi kD}\left\{ W(u) + f\left(u,\frac{r}{D},\frac{b}{D},\frac{d}{D},\frac{z}{D}\right)\right\} \qquad (1.5)$$

where

$$W(u)=\int_{\xi=u}^{\infty}\frac{e^{-\xi}d\xi}{\xi},$$

and

$$f=\frac{2D}{\pi(b-d)}\sum_{n=1}^{\infty}\left\{\frac{1}{n}\left(\sin\frac{n\pi b}{D}-\sin\frac{n\pi d}{D}\right)\cos\frac{n\pi z}{D}\,W\left(u,\frac{n\pi r}{D}\right)\right\}$$

where

$$u=\frac{r^2S}{4tkD}$$

and

$$W\left(u,\frac{n\pi r}{D}\right)=\int_{\xi=u}^{\infty}\frac{1}{\xi}\exp\{-\xi-\frac{(\frac{n\pi r}{D})^2}{4\xi}\}d\xi$$

ξ is a dummy variable.

If s is not observed at a point z, but over an interval b' to d' (Figure 12), s has to be integrated over the observed interval, hence;

$$f_m\left(u,\frac{r}{D},\frac{b}{D},\frac{d}{D},\frac{b'}{D},\frac{d'}{D}\right)=\frac{2D^2}{\pi^2(b-d)(b'-d')}\cdot\mathbf{B} \qquad \textbf{(1.10)}$$

where

$$\mathbf{B}=\sum_{n=1}^{\infty}\frac{1}{n^2}(\sin\frac{n\pi b}{D}-\sin\frac{n\pi d}{D})(\sin\frac{n\pi b'}{D}-\sin\frac{n\pi d'}{D})W(u,\frac{n\pi r}{D})$$

If $b'-d' < 0.05\cdot D$, the difference between f and f_m is negligible.

If u is small, then f and f_m can be considered stationary, and is only a function of the position.

Hantush (1961) claims that if

$$u < \frac{1}{20}\left(\frac{\pi r}{D}\right)^2$$

then $W(u,n\pi r/D)$ can be approximated very closely by $2K_o(n\pi r/D)$ where K_o is the zero-order modified Bessel-function of the second kind.

The most important anisotropy at Haslemoen is the difference between vertical and horizontal hydraulic conductivities. In such cases anisotropy can be taken into account by letting f, that include vertical flow, be a function of the radius multiplied by the ratio of vertical to horizontal conductivity $\beta = r/D \cdot (k_z/k_h)^{1/2}$ (Kruseman and de Ridder, 1992). Then (1.5) is reduced to

$$s(r,z,t) = \frac{Q_w}{4\pi k_h D}\left\{ W(u) + f_s\left(\beta, \frac{b}{D}, \frac{d}{D}, \frac{z}{D}\right)\right\} \qquad \textbf{(1.13)}$$

where

$$f_s = \frac{4D}{\pi(b-d)}\sum_{n=1}^{\infty}\left\{\frac{1}{n}K_0(n\pi\beta)\left(\sin\frac{n\pi b}{D} - \sin\frac{n\pi d}{D}\right)\cos\frac{n\pi z}{D}\right\}$$

Or if s is observed over an interval b' to d';

$$f_{ms}\left(\beta, \frac{b}{D}, \frac{d}{D}, \frac{b'}{D}, \frac{d'}{D}\right) = \frac{4D^2}{\pi^2(b-d)(b'-d')} \cdot \mathbf{B}' \qquad \textbf{(1.15)}$$

where

$$\mathbf{B}' = \sum_{n=1}^{\infty}\frac{1}{n^2}K_0(n\pi\beta)\left(\sin\frac{n\pi b}{D} - \sin\frac{n\pi d}{D}\right)\left(\sin\frac{n\pi b'}{D} - \sin\frac{n\pi d'}{D}\right)$$

One important practical result from Hantush (1961) is that at a radius r greater than $1.5 \cdot D \cdot (k_h/k_v)^{1/2}$ to $2 \cdot D \cdot (k_h/k_v)^{1/2}$ the flow is essentially 2 dimensional and the f-part can be neglected in equation 1.13.

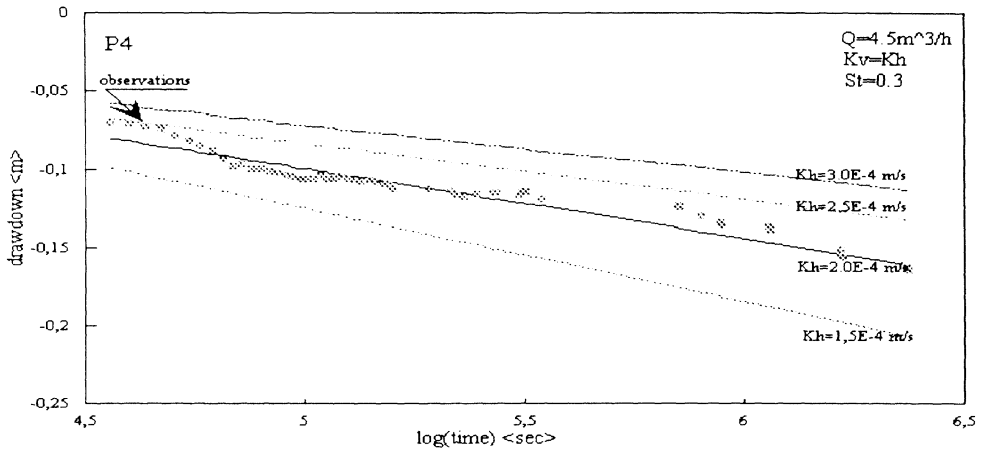

Figure 20. *Observed and simulated drawdown at P4 (Figure 13). Only horizontal conductivity is allowed to vary. Kv=Kh means isotropic conditions.*

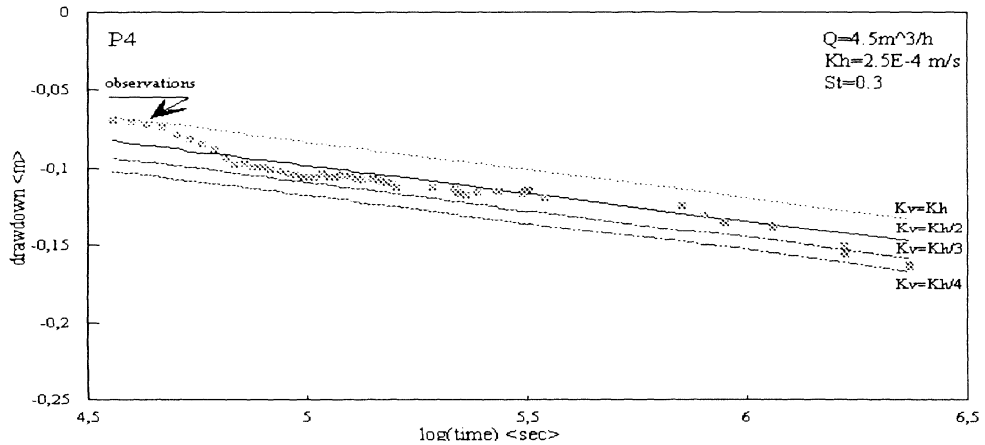

Figure 21. *Observed and simulated drawdown at P4 (Figure 13). Only vertical hydraulic conductivity is allowed to vary.*

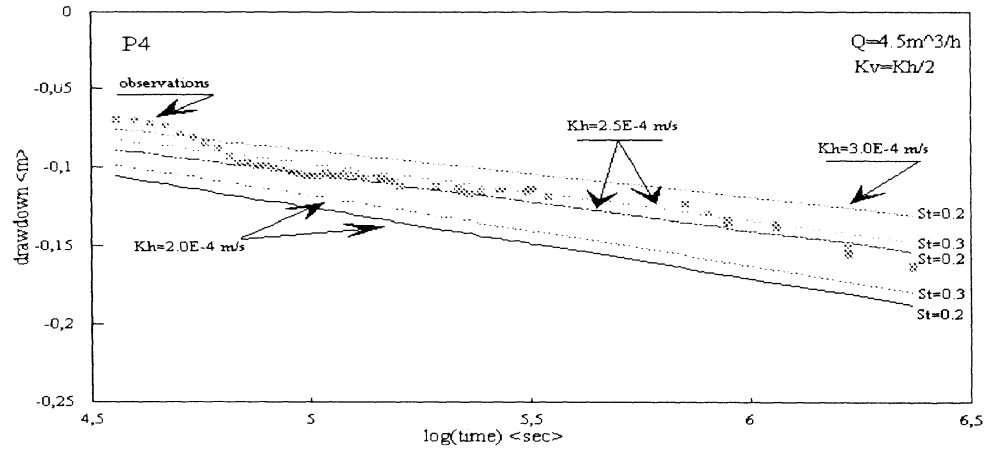

Figure 22. *The simulations show that drawdown at P4 (Figure 13) is not very sensitive to variation of storativity.*

Calibration and sensitivity analysis

To simulate drawdown we needed to write subroutines in order to calculate $W(u)$, f_s, f_{ms} and K_o. All subroutines were controlled against tabulated functions (see app. and e.g. Bear, 1979 or Kruseman and de Ridder, 1992). From these subroutines we calculated the drawdown in each of the observation wells. For each well k_h, k_v and S is tuned to fit the observations as shown in Figure 20, Figure 21 and Figure 22 for P4.

The simulation indicated following ranges for k_h, k_v and S:

$$2.0 \cdot 10^{-4} < k_h < 2.5 \cdot 10^{-4} m/s$$

$$k_h < k_v < \tfrac{1}{2} k_h$$

$$0.2 < S < 0.3.$$

Finally we used one set of parameters to simulate the observed drawdown in all wells. In Figure 23 are drawdown simulated in P3, P4 and G3 with parameters; $k_h=2.0 \cdot 10^{-4} m/s$, $k_v=1.5 \cdot 10^{-4} m/s$, and $S=0.20$. At a radius less than 2 m the assumption of using the equations for a confined aquifer is not fulfilled, and we were not able to simulate the drawdown with desired precision. At a radius less than 2 m the observed drawdown is always less than simulated. At P1 (radius of 0.3 m) observed drawdown is 30-40 cm less than simulated. Generally the simulations indicate more drawdown than observed at P1, P2, P3 and P4, but underestimate drawdown at G3 (see Figure 24 where accumulated deviation between simulated and observed drawdown is plotted).

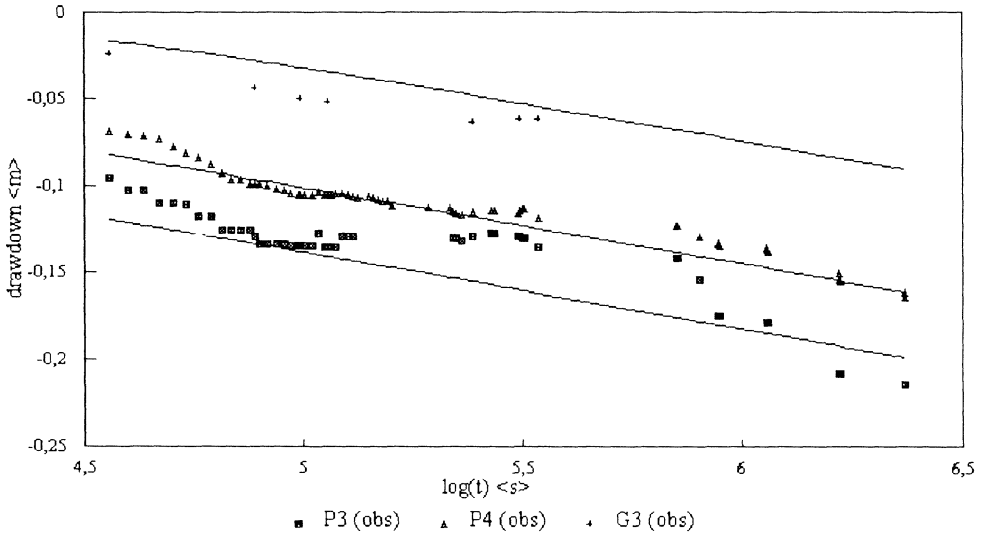

Figure 23. *Observed and simulated drawdown at P3, P4 and G3 (Figure 13). Parameters are; $k_h=2.0$, $k_v=1.5$, both 10^{-4}m/s, and St=0.2*

At a radius of 30 m the flow is close to 2 dimensional, and observations can be fitted to a Theis type-curve. This gives estimates of k_h and S in the range of $1.5 \cdot 10^{-4} < k_h < 2.0 \cdot 10^{-4} m/s$ and $0.2 < S < 0.3$.

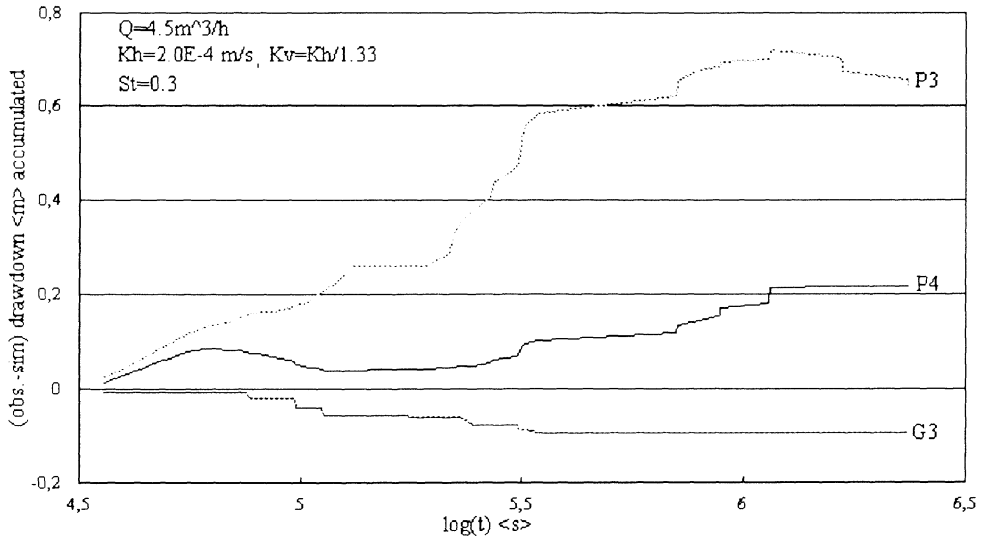

Figure 24. *Accumulated deviation between simulated and observed drawdown at P3, P4 and G3 (Figure 13). Over estimation in P3 and P4, under estimation in G3.*

Break-through simulation

After obtaining one set of parameters, flow in the horizontal and the vertical directions were calculated analytically in a 25 x 25 cm grid net, 12 m in the radial- and 12 m in the z-direction (Figure 25). These flow fields were imported to 'ASM' (Kinzelbach and Rausch, 1989) where a 'random-walk' algoritme was utilized to simulate break-through curves.

70% of the recovered tracer appeared in Q2 (Figure 26). We are not able to simulate the break-through curves in all the three pumping-wells assuming a homogeneous aquifer. So at this stage we are satisfied with simulating the break-through in Q2.

In the following simulations we assumed no adsorption, as this quantity is uncertain. The retardation factor was then set to 1. However, the average velocity of a moving tracer depends heavily on adsorption. The greater the adsorption factor, the greater is the retardation of the moving tracer. This means that the front moves slower than the average pore flow velocity. If the break-through time is monitored, pore flow velocities have to be increased by a decreasing effective porosity to balance an increasing adsorption factor. If we assume no adsorption, the tracer

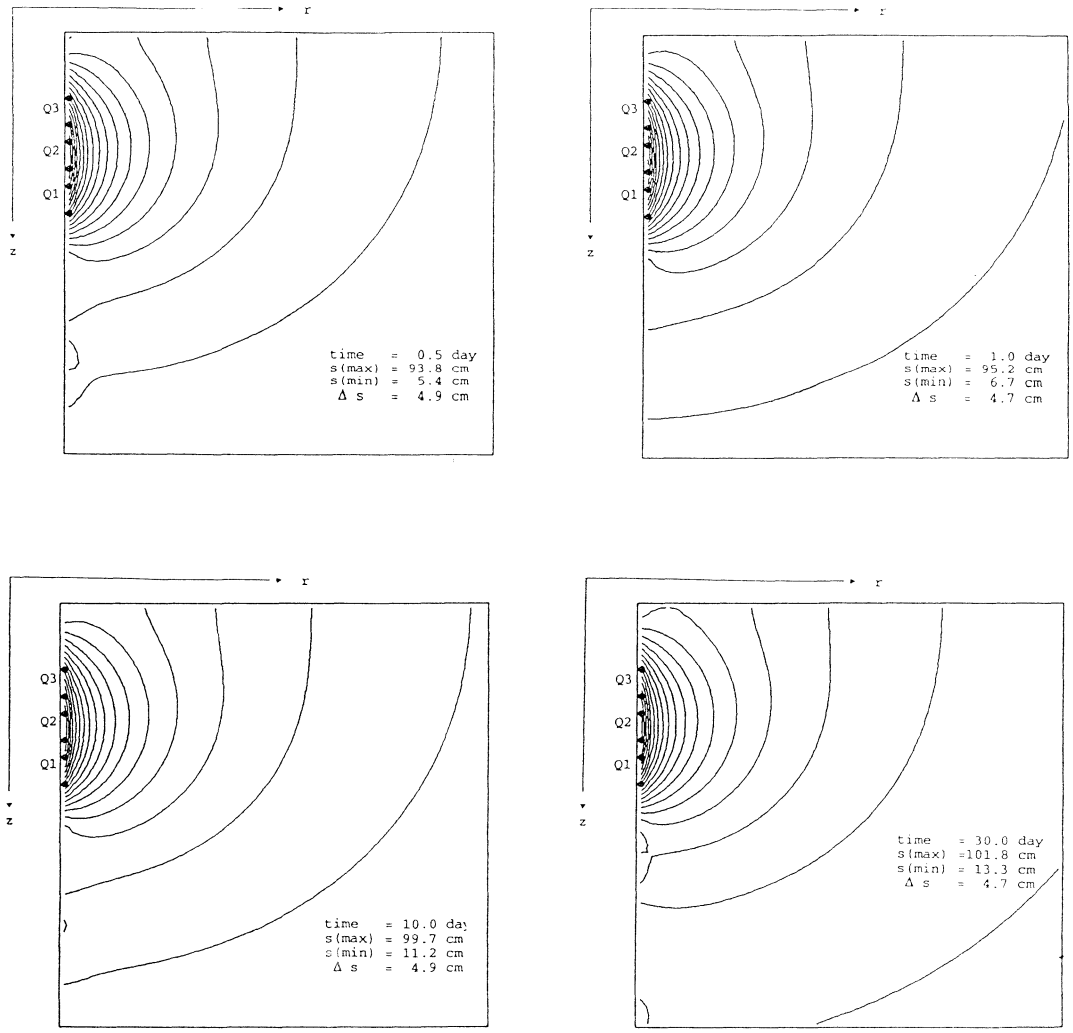

Figure 25. *Drawdown simulation after ½, 1, 10 and 30 days of pumping in the interval; 0≤r≤12 m and 0≤z≤12 m. The thickness of aquifer is 25 m.*

front would have the same velocity as the pore water. The estimates of effective porosity have therefore to be considered as maximum estimates.

Head distribution after 10 days of constant pumping was calculated (***Q3=0.444 l/s, Q2=0.405 l/s, Q1=0.400 l/s***). With horizontal and vertical hydraulic conductivities of ***2.0 · 10^{-4}m/s*** and ***1.5 · 10^{-4}m/s*** respectively, effective porosity of ***26.63 %***, longitudinal and transversal dispersivity of ***3 cm*** and ***0 cm*** respectively. Breakthrough was simulated to ***6.9 days*** with the maximum concentration after ***9 days*** (Figure 27). The injection of tracer was set to 11.25 m away from the pumping tubes, that is 1 m more than the actual radial distance between injection- and pumping tubes. This was done to compensate for the additional drift caused by the regional groundwater flow (Figure 13).

At 8 days after the injection there was a small interruption in pumping at Q1 and Q2 while pumping was continued in Q3. This caused a temporarily decrease in Rhodamine concentration in Q2. Without this interruption in pumping the break-through curve at Q2 would have been smoother and the previous increase in concentration would probably have been continued, and the whole concentration curve shifted somewhat to the left. Accordingly we allow the simulated maximum concentration to occur a little bit earlier than the observed maximum in Q2.

The greatest deviation between observed and simulated curves occur in the recession. The most likely explanation to this discrepancy is the numerous breaks in pumping due to maintenance and techniqual problems. Every stop in pumping will cause a drift of tracer due to the regional flow gradient. Two physical reactions that most likely plays a role in this case, is the following: When the concentration of the tracer is high, a strong adsorption of tracer to matrix may occur. After a while, when the concentration of the tracer declines, the adsorbed tracer may dissolve and start to move towards the pumping tube again after having been retained in the matrix for a while. This may be looked upon as a secondary internal source. The effect will be an extended recession of tracer at the pumping tubes. Another important factor is inhomogeneities in the aquifer. When the concentration of tracer is high a diffusion may take place from a permeable unit into a less permeable unit. After a while, when the concentration of tracer is less in the permeable unit as a result of advection, the diffusion will go the opposite way. This effect will also contribute to a skewness in break-through curves (Sudicky, 1986).

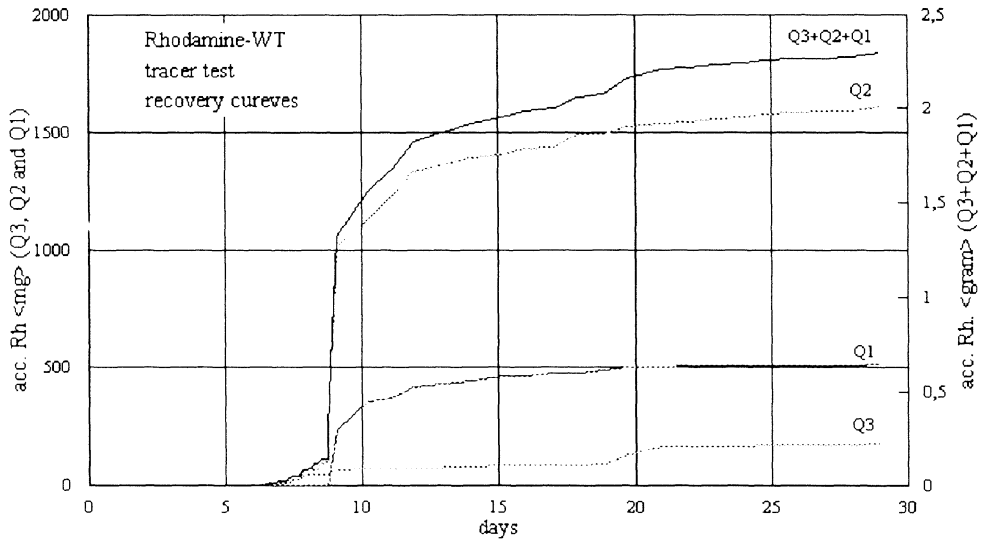

Figure 26. *Accumulated recovery of Rhodamine-WT in the pumping wells. Of 43.43g injected Rh-WT was only 2.3g recovered.*

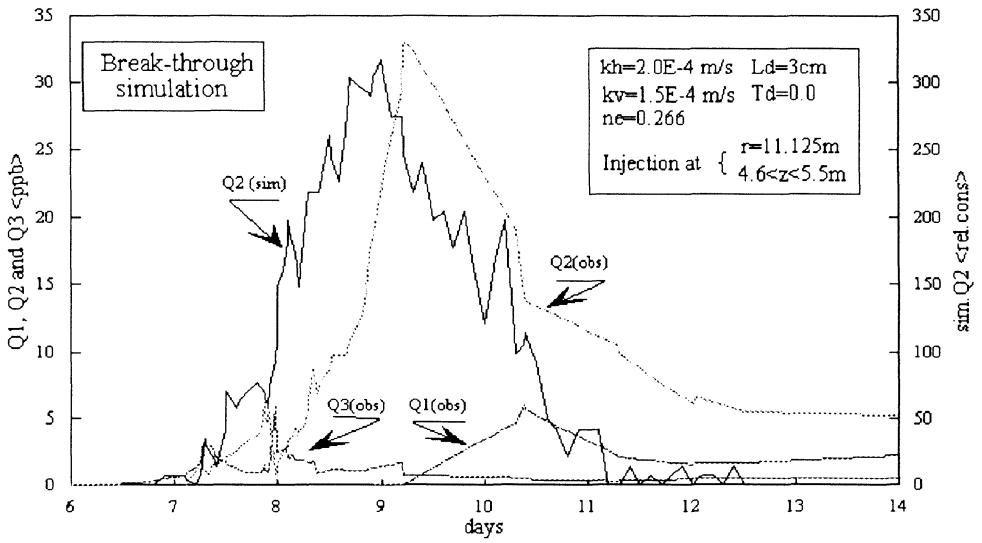

Figure 27. *Break-through simulation of Rhodamine-WT . In this simulation adsorption was neglected and retardation factor was set to 1.*

6.2 Numerical simulation with the fluid dynamics analysis package FIDAP

In order to simulate the propagation of a tracer through the aquifer a numerical model was used. The model uses the finite element method and is a commercially available fluid dynamics analysis package, FIDAP (1991), designed for a wide range of fluid problems. It can handle both linear and nonlinear fluids, porous flow, stationary or transient modes, and two or three dimensional modes with complicated boundary conditions. The main advantage with the finite element method, compared to e.g. the finite difference method, is the great flexibility in the element mesh. An aquifer with complicated topography can easily be discretized and the same aquifer can be divided in different element groups where each group represents geological units with different petrophysical parameters.

At this stage we have only simulated the tracer test under the same geological assumptions and hydraulic conditions as for the analytical model. This was necessary to make sure that FIDAP and the analytical solution calculated the same flow field. A next step will be to include element groups in FIDAP that represent a more realistic aquifer. When future aquifer evaluations take place (e.g. Upper Romerike), this model can easily be modified to fit new geologic and hydraulic conditions.

Mathematical model

FIDAP solves the Navier-Stokes equation for incompressible viscous flow in a broad sense. In the following the equations of flow in a isothermal saturated media

are outlined. The reader is referred to Bear (1972) for a complete discussion on the derivation and validity of these equations.

Suppose that within the domain of interest Ω there is a region V containing a rigid porous material saturated with a viscous incompressible fluid. In FIDAP the domain Ω can also consist of a region Ω_f occupied entirely by fluid. The saturating fluid in V must be the same as in Ω_f if the two regions share a common permeable interface. In this work, however, Ω is entirely occupied by V.

Assuming that the porous medium is homogenous and isotropic and the fluid and the solid are in thermal equilibrium, then the equations describing the fluid motion in the region V are as follows. Within V, let V_f be the volume occupied by the fluid and V_s the volume occupied by the solid, where

$$V = V_f + V_s$$

The porosity of the porous medium is defined by

$$n_e = \frac{V_f}{V}$$

To derive the porous flow equations two averaged quantities are introduced;

$$V_m = \frac{1}{V}\int_{V_f} v\,dV$$

and

$$V_n = \frac{1}{V}\int_{V} v\,dV$$

where v is any quantity (scalar, vector or tensor). v_m is referred to as the pore average and v_h as the volume average of the quantity v. v_m and v_h are related by $v_h=n_e v_m$. In particular, the volume averaged velocity u_i and pressure p of the fluid is defined by

$$u_h = \frac{1}{V}\int_{V} u_i\,dV$$

Omitting the index h on the averaged values and following the convention used

$$p_h = \frac{1}{V}\int_V p\,dV$$

in groundwater modelling, u_h is similar to the Darcy velocity $\boldsymbol{q}$. Performing the volume average of the momentum and continuity equations results in the following equations.

Momentum:

$$\frac{\rho}{n_e}\frac{\partial \boldsymbol{q}}{\partial t} + \left\{\frac{\rho c_c}{\sqrt{\kappa_i}}\|\boldsymbol{q}\|^m + \frac{\mu}{\kappa_i}\right\}\boldsymbol{q} = -\nabla p + \nabla\cdot\left\{\mu_e(\nabla \boldsymbol{q} + \nabla \boldsymbol{q}^T)\right\} + \rho \boldsymbol{f}$$

Continuity:

$$\nabla \cdot (\rho q_i) = 0$$

where ρ is the density of the fluid, n_e is the porosity, κ_i is the permeability[1], c_c is the inertia coefficient, μ and μ_e is viscosity and an effective viscosity and $\|\boldsymbol{q}\|$ is the magnitude of the velocity. p is pressure and f is external forces, in this case the gravitational acceleration.

The equations presented above represent a generalization of the standard Darcy equations for isothermal flow in a saturated porous medium. This system is sometimes referred to as the Forchheimer-Brinkman model for porous flow.

Regarding the momentum equation given above it can be seen that this is very similar to the standard momentum equation in the Navier-Stokes equations. The difference being basically the two terms in brackets on the left side.

The first of these terms is derived from the convective term $(\boldsymbol{q}\cdot\nabla\boldsymbol{q})$ in the standard Navier Stokes equation. This term is often referred to as the Forchheimer term and is an inertia term due to local accelerations. The second term is the standard Darcy approximation of the viscous force (pr. unit volume) which resists the motion. When the local Reynolds number is less than 1 the Forchheimer term will be very small compared to the Darcy term and may therefore be neglected.

[1]The most general form of the permeability κ is a tensor κ_{ij}. In FIDAP it is assumed that the off-diagonal terms of this permeability tensor are zero; thus, the principal axes of the permeability tensor must coincide with the coordinate axes.

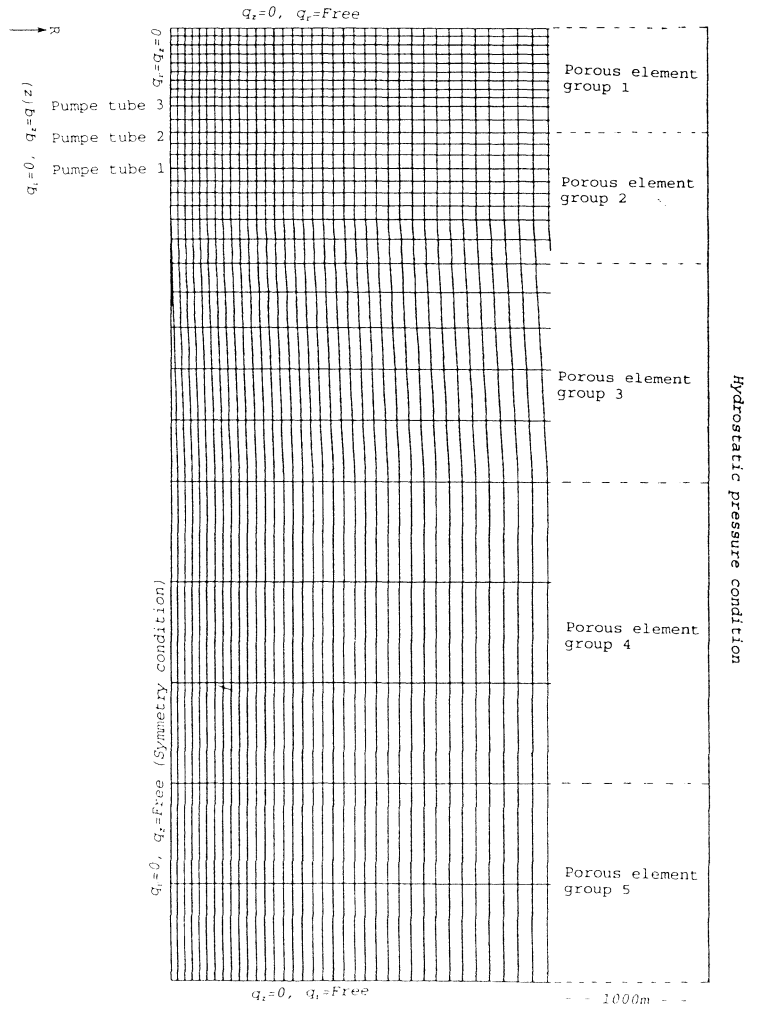

Figure 28. *Boundary conditions and mesh used in the FIDAP simulation. Dirichlet boundary condition at r=1000 m.*

Because of the similarities between the standard Navier-Stokes equations and the equations given above, it is quite straightforward to combine a porous medium and a general flow region in a given flow simulation. A model for this flow situation is often referred to as a Brinkman model.

Regarding the general momentum equation given above it can be noted that by judicious selection of the various coefficients, a number of standard flow models can be derived. Thus if $c_c=0$, a Brinkman model is obtained, while if $\mu_e=c_c=0$, the standard Darcy formulation is approached. For a further discussion of individual models and their regions of applicability, the reader is referred to Bear (1972).

From the above we can conclude that a stationary Darcy formulation will be identical with the potential approach used in the analytical solution. The only

exception is that the permeability is included in the Darcy term, while the so called hydraulic conductivity appears in the potential formulation. These parameters are related by

$$k = \kappa \frac{\rho g}{\mu}$$

where g is the gravitational acceleration.

On each segment of the boundary of the computational domain Ω it is necessary to prescribe appropriate boundary conditions. The boundary condition relating to the momentum equation is either the specification of velocity components:

$$q_i = q_i(\zeta)$$

or specification of surface stresses:

$$\sigma_i = \sigma_{ij} n_j(\zeta) = \sigma_i(\zeta)$$

where σ_{ij} is the stress tensor and ζ is a parameter measuring position along the relevant boundary segment. $n_j(\zeta)$ is the outward unit normal to the boundary.

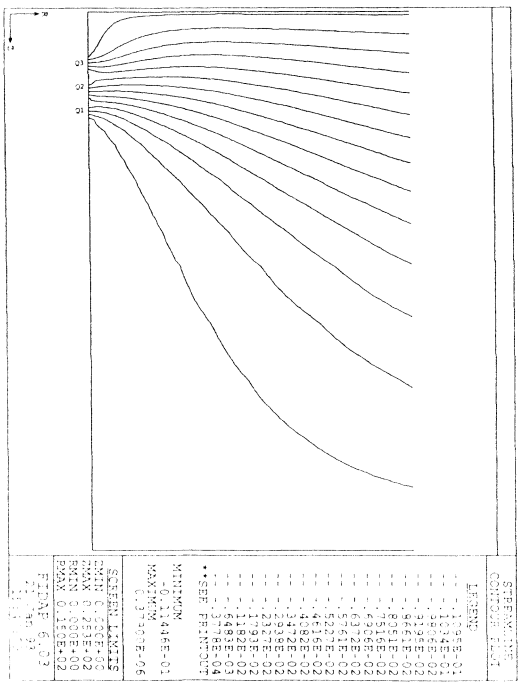

Figure 29. *Streamlines between; 0<r<15m and 0<z<25.3m. The flowrate is the difference between two streamlines.*

The surface of the aquifer is considered to be fixed in space (confined aquifer) and the boundary conditions on the surface are given by velocities. As shown in Figure 28 velocity boundary conditions are also given on the bottom and on the side near the pumping tubes. A hydrostatic pressure condition is specified on the boundary far from the pumping tubes. At the pumping tubes a parabolic velocity profile was specified and adjusted until the correct flowrate was obtained. Subject to these boundary conditions the equations of mass and momentum conservation were solved in an axisymmetric coordinate system.

Numerical results and experiences

The drawdown s, is very small compared to the thickness of the aquifer. The numerical simulation is therefore very sensitive both to boundary conditions and to the discretization of the flow field. The problem of boundary conditions is mainly connected to how far from the pumping tubes we may claim that hydrostatic pressure exists. In the numerical model it was necessary to set this distance to approximately 1000 m in order to get the correct drawdown. In the analytical solution constant head was at infinity.

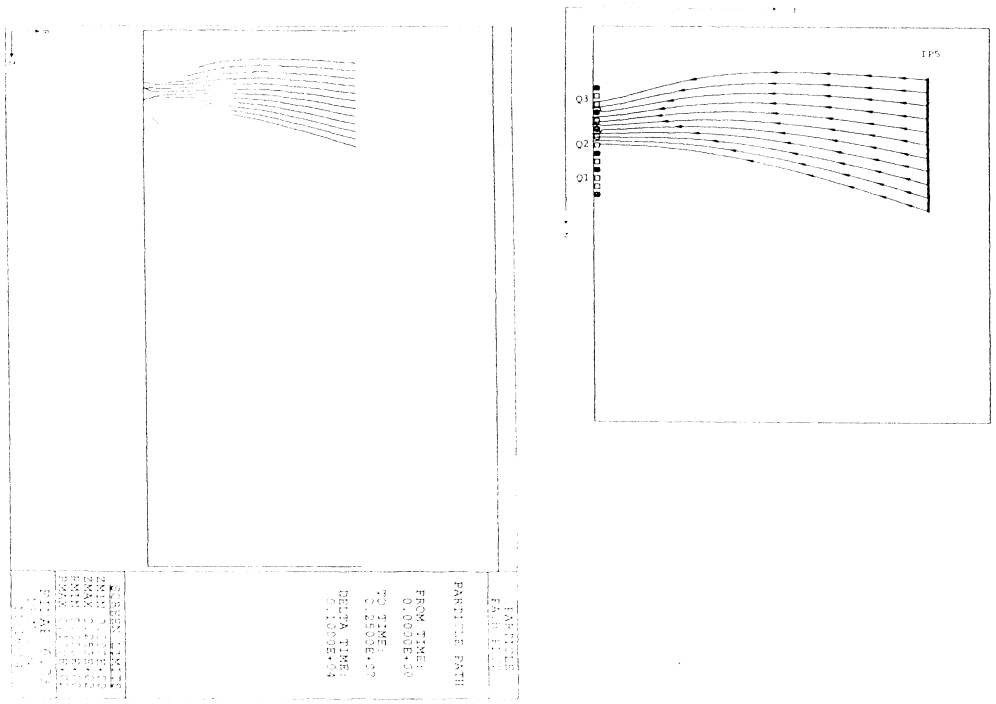

Figure 30. *Tracer simulation with Darcy velocity and advection. FIDAP to the left, and the analytical model to the right (marker each 5th day travel).*

Figure 29 shows the streamlines in the region near the pumping tubes. This flow-field is seen to be very similar to the field calculated by potential theory. Figure 30 shows the transport pattern of twelve massless particles after approximately 29 days. It can be seen from the plot that the tracer first enters the middle pumping tube, Q2. This occur because we (so far) assume homogeneity. In reality the break-through occurs first in the upper well (Q3) because there is a slightly decreasing permeability with depth. In this simulation the tracers are transported by pure advection and the velocity is the volume average velocity (Darcy velocity). Imposing the same effective porosity (0.27) as we used in the simulation with the analytical model the break-through would occur at 7.8 days. (29 days multiplied by the effective porosity of 0.27)

As mentioned above the numerical simulations are not yet completed. The most interesting part still remain, that is to evaluate the relative impact from different geological units to the drawdowns and the break-through times. It is our intention to continue this work with FIDAP.

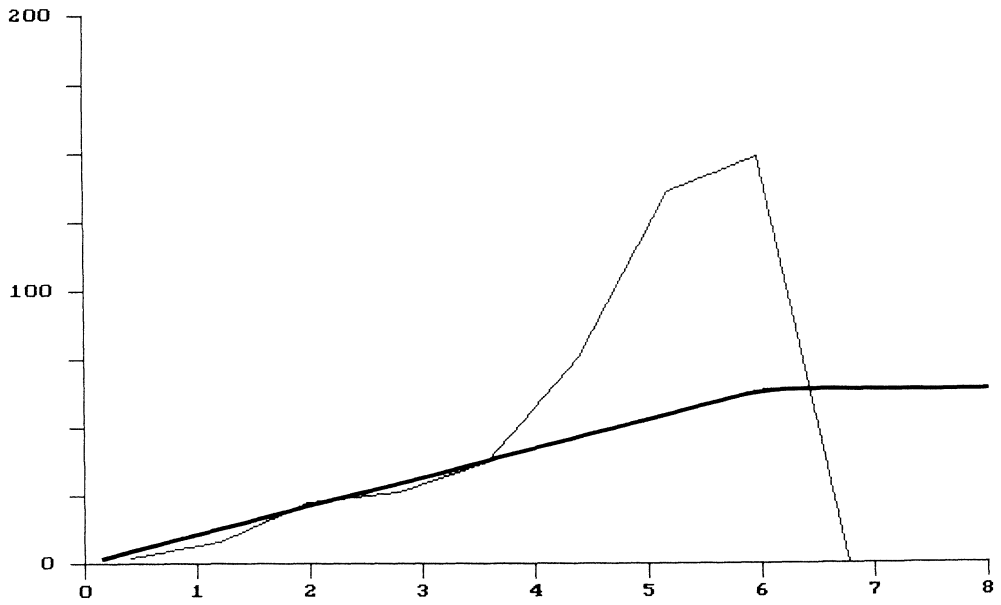

Figure 31. *Fitted linear semivariogram (bold) to experimental semivariogram (light). Range at 6 km (x-axis) and sill at 65 m^2.*

7 Geostatistical analysis of groundwater levels

One standard objective of geostatistical analysis is to estimate the value of the variable under study (here groundwater levels), z in the point x_o, as a linear combination of regional observations $z(x_i)$; $i=1,...,n$. The estimator is therefore:

$$z^*(x_0) = \sum_{i=1}^{n} \lambda_i z(x_i) = \mathbf{\Lambda}^T \mathbf{Z}$$

where $\mathbf{Z}$ is the column vector of observations and Λ^T is the transposed column vector of weights λ_i, $i=1,...,n$ associated to the observations. Optimal weights can be found, based on the intrinsic assumption and under the conditions of unbiasedness, by minimizing the estimation variance. This gives rise to the system of kriging equations that read in the matrix notation:

$$\mathbf{\Gamma}\,\mathbf{\Lambda} = \mathbf{\Gamma}_0$$

where

$$\mathbf{\Gamma} = \begin{Bmatrix} \gamma(0) & \gamma(|x_1-x_2|) & \cdots & \gamma(|x_1-x_n|) & 1 \\ \gamma(|x_2-x_1|) & \gamma(0) & \cdots & \gamma(|x_2-x_n|) & 1 \\ \cdot & \cdot & \cdots & \cdot & \cdot \\ \cdot & \cdot & \cdots & \cdot & \cdot \\ \cdot & \cdot & \cdots & \cdot & \cdot \\ \gamma(|x_n-x_1|) & \gamma(|x_n-x_2|) & \cdots & \gamma(0) & 1 \\ 1 & 1 & \cdots & 1 & 0 \end{Bmatrix}$$

$$\mathbf{\Lambda} = \begin{Bmatrix} \lambda_1 \\ \lambda_2 \\ \cdot \\ \cdot \\ \cdot \\ \lambda_n \\ \mu \end{Bmatrix} \quad \textit{and} \quad \mathbf{\Gamma}_0 = \begin{Bmatrix} \gamma(|x_1-x_0|) \\ \gamma(|x_2-x_0|) \\ \cdot \\ \cdot \\ \cdot \\ \gamma(|x_n-x_0|) \\ 1 \end{Bmatrix}$$

$\gamma(\boldsymbol{h})$ denotes the (point) semivariogram for the distance $\boldsymbol{h}$ and $\boldsymbol{\mu}$ is the Lagrange multiplier.

A theoretical semivariogram (or correlation function) determined for all data is subsequently used to estimate parameter values and kriging variances for every observational point. Linear, spherical, exponential and Gaussian models (Clark, 1979) are used in the present study as theoretical semivariograms.

The empirical semivariogram is determined from the experimental data set for the event t_k by the equation:

$$\hat{\gamma}_k(h) = \frac{1}{2N(h)} \sum_{(i,j)\in R(h)} \{ z(x_i,t_k) - z(x_j,t_k) \}^2$$

where

$$R(h) = \{ (i,j); h - \varepsilon \le |x_i - x_j| \le h + \varepsilon \}$$

that is, all pairs of sites separated by a distance close to h are considered, and $N(h)$ is the number of elements in the distance class $R(h)$. Figure 31 shows the empirical semivariogram and a fitted linear theoretical one. In the procedure of fitting the theoretical semivariogram the main weight has been restricted to the left hand side of the diagram, which represents typical distances between observation points. The empirical semivariogram is not very accurate at large distances.

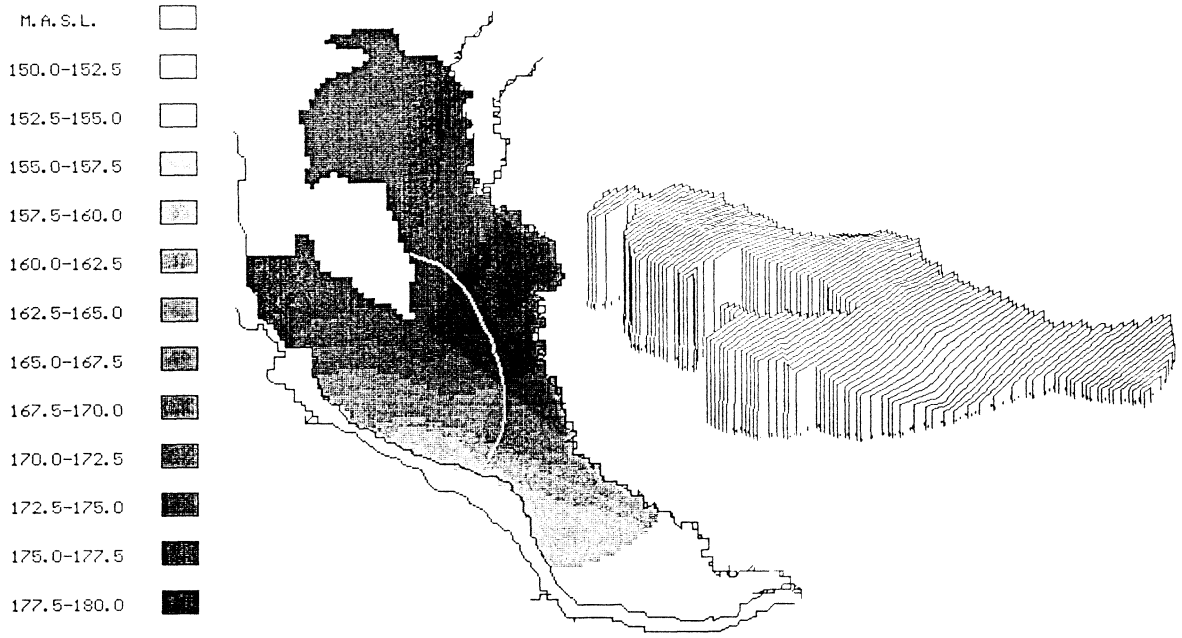

Figure 32. *Estimated groundwater table by kriging. 3D-plot to the right. The white line is the modelled flow path (chapter 8).*

A cross-validation (i.e. each observation point is successively excluded from the analysis and forecasted from neighboring observations) was performed on groundwater level data from 31 tubes on four occasions. Results from one of them (Nov 1989) is shown in Tabell III. There is a very good agreement between the observed and estimated groundwater levels. The deviation is only in one case larger than the one expected from the theoretical estimation error. The results are almost identical for the four different occasions.

Figure 32 shows the estimated groundwater table for the event of Nov 1989 and Figure 33 the corresponding estimation error. We can note that no information from the levels of the Glomma and Hasla rivers has been used. That is why the estimation errors are rather large along these. This will be improved.

The interpolation routines have been combined with a Geographical Information System IDRISI. In this are stored digital terrain models of geological formations and the interpolated groundwater levels. From this flow paths can be traced automatically (Figure 32), and information on the aquifer geometry along the corresponding section, can be retrieved.

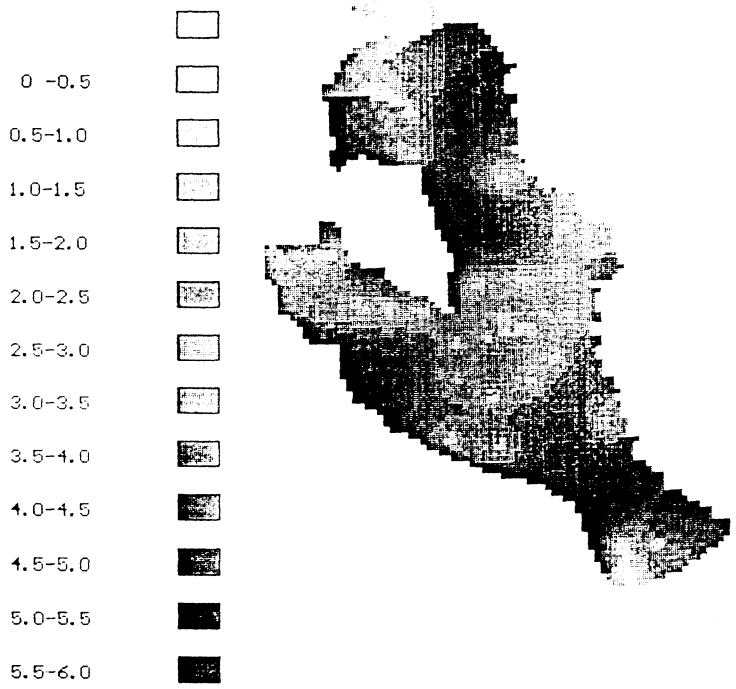

Figure 33. *Estimation error connected to the kriged groundwater table (Figure 32). The scarcity of data along Glomma and Hasla cause large estimation error.*

Table III Cross-validation with linear semivariogram model, nugget=0, sill=65 m^2, range=6.0 km

St.nr.	Observed	Estimated	Estimation error	nn	Sign.
1	167.95	164.65	2.71	22	
2	163.80	163.19	3.68	19	
3	167.38	167.10	2.55	23	
4	170.77	171.24	1.08	26	
5	172.29	172.06	2.59	27	
6	155.84	162.09	2.55	21	*
7	170.62	170.50	2.37	26	
8	171.83	172.15	2.80	25	
9	171.75	170.89	2.61	23	
10	168.86	170.97	2.34	17	
11	170.04	170.72	2.00	26	
12	171.22	171.61	1.85	27	
13	170.69	170.83	2.04	27	
14	169.38	169.85	2.35	25	
15	168.65	168.49	2.43	23	
16	168.63	167.22	2.64	23	
17	172.98	172.73	3.05	28	
18	171.98	170.09	2.67	20	
19	179.22	178.14	1.82	5	
20	155.72	160.36	2.56	3	
21	169.42	168.98	2.32	24	
22	170.82	171.42	1.46	26	
23	178.85	177.72	3.53	11	
24	173.12	173.72	3.74	19	
25	157.16	160.20	3.18	21	
26	168.98	170.13	1.80	19	
27	172.14	172.45	2.49	23	
28	176.80	175.02	3.16	10	
29	173.31	172.86	2.46	17	
30	171.89	170.84	1.20	26	
31	170.72	170.55	1.30	26	

8 Regional groundwater flow

Modelling of regional groundwater flow at Haslemoen has been through several stages. Preliminary 2-D models in the horizontal plane have been calibrated (Einan, 1989 and Kitterød, 1991). These models have to be considered as insufficient because of scarcity of data. None of the presented models so far include the results from the geostatistical analysis presented in the previous chapter.

Through this project we have sampled additional hydrological and geological data (Table I). With the help of these data we was able to calibrate and validate a 2-D flow model in the vertical plane along one streamline (Figure 32). This was done before the new geological model of the aquifer was completed.

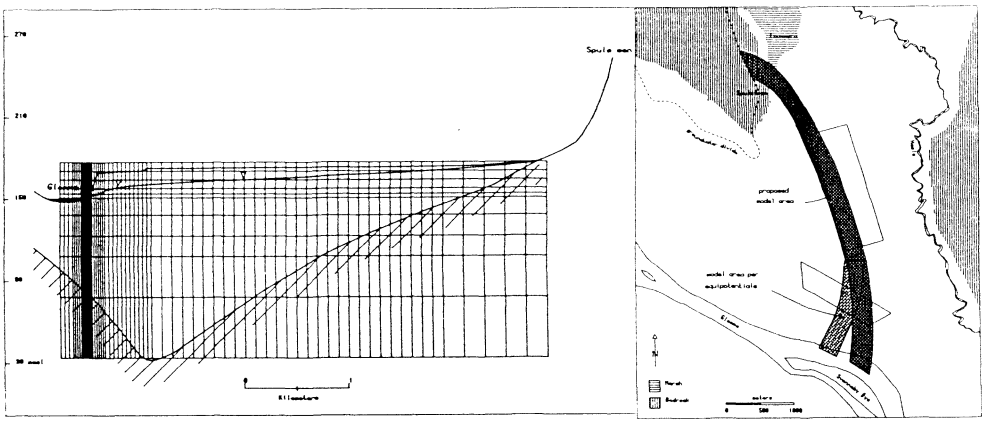

Figure 34. *The model grid used in MODFLOW (left) and the flow-path modelled in 2D (right), Allen (1992).*

'A Modular Three-Dimensional Finite-Difference Groundwater Flow Model' (MODFLOW, McDonald and Harbaugh, 1988) was run in a 10 x 70 grid system (Figure 34). With recharge set to 0.8 mm/day (288 mm/year) the model was calibrated for a steady state flow to a subset of observed data with values of K_h and K_v listed in Table IV. To simulate the heads close to Glomma properly, we had to introduce a local heterogeneity in layer 5.

Table IV K_h and K_v <m/s> for steady state calibration (Allen, 1992)

Layer	K_h	Layers	K_v
1	$2.3 \cdot 10^{-4}$		
2	$2.3 \cdot 10^{-4}$	1-2	$5.6 \cdot 10^{-5}$
3	$2.3 \cdot 10^{-4}$	2-3	$5.6 \cdot 10^{-5}$
4	$2.3 \cdot 10^{-4}$	3-4	$5.6 \cdot 10^{-5}$
5	$2.3 \cdot 10^{-4}$	4-5	$5.6 \cdot 10^{-5}$
6	$7.2 \cdot 10^{-5}$	5-6	$2.4 \cdot 10^{-6}$
7	$1.2 \cdot 10^{-6}$	6-7	$6.9 \cdot 10^{-7}$
8	$1.2 \cdot 10^{-6}$	7-8	$6.9 \cdot 10^{-8}$
9	$1.2 \cdot 10^{-7}$	8-9	$4.2 \cdot 10^{-9}$
10	$1.2 \cdot 10^{-8}$	9-10	$2.8 \cdot 10^{-10}$

From the remaining data subset the model was validated (Figure 35). The minor off-set between observed and simulated data is most likely due to the Dupuit assumption. Close to Glomma there is a strong vertical vector in groundwater flow. Sensitivity of head to river stage and recharge shows three zones of influence. In the first area adjacent to Glomma (0-30 m from riverside) the river stage overrides the effect from recharge. In the second area (30-70 m) recharge and the river stage of approximately equal significance. In the third area, more than 70 m from the river, Glommas influence on the head is negligible. In the observation period (May 1990 to August 1991) the flow direction of the groundwater was always towards the river. Even if the groundwater head adjacent to Glomma is determinated by river stage, the groundwater was always flowing towards the river at Haslemoen. For further details see Allen, 1992.

Based on the geological framework discussed in chapter 5 we designed another 2-D vertical flow model. This model is not yet fully calibrated, but we include some results from this preliminary modelling work to illustrate the impact from the geological framework on flow and residence time.

A finite difference code (Aquifer Simulation Model - 'ASM', Kinzelbach and Rausch, 1989) was run basically along the same stream lines as the previous model (Figure 32). The aquifer was discretized by a 60 x 60 grid net over a distance of 5000 m x 150 m. Close to the river side, the grid size was 25 m x 1

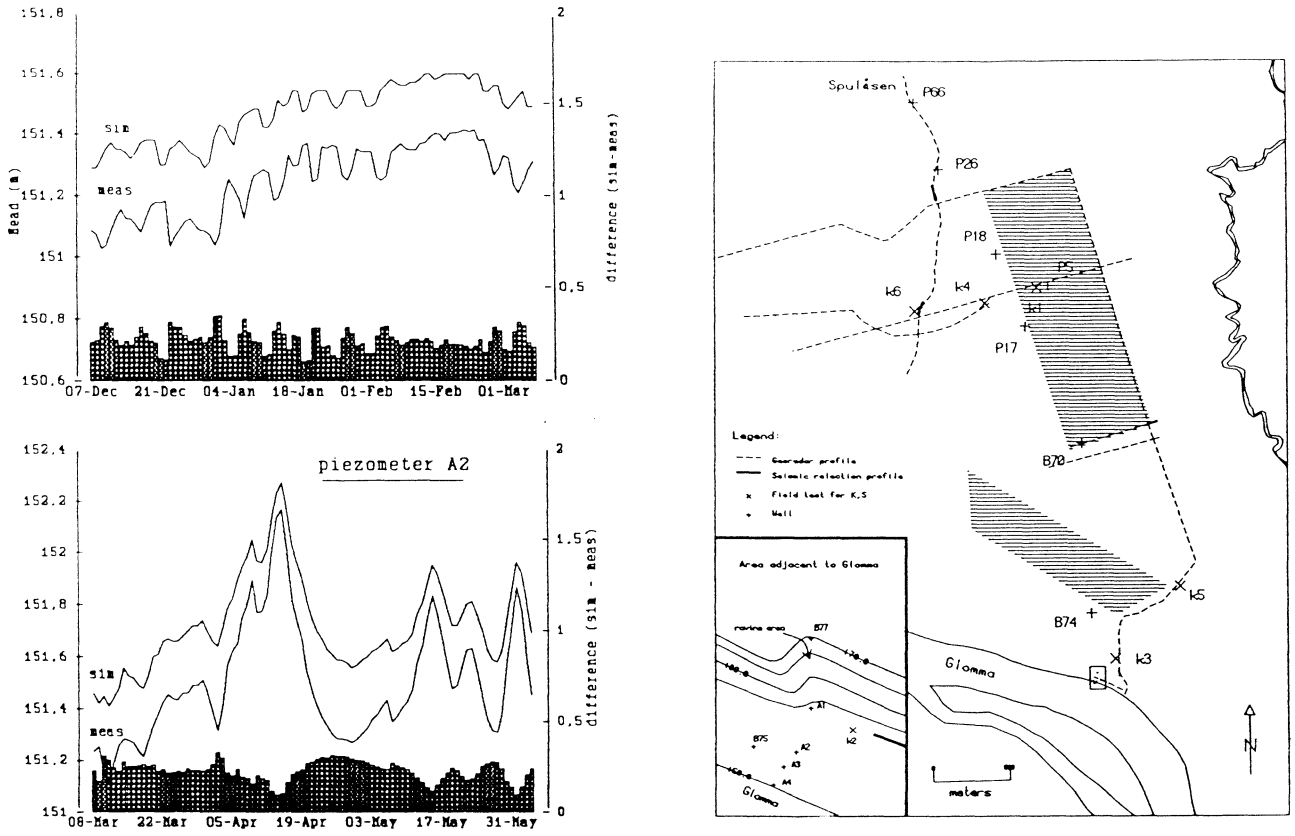

Figure 35. *Simulated vs. measured head levels in piezometers A1 and A2 (left). Location map to the right, Allen (1992).*

m (the stream tube was set to 100 m width).

Our primary objective so far, has been the steady state flow. Accordingly we can allow the groundwater table to be a fixed surface. By doing so, the aquifer can be considered as confined. The groundwater level is fluctuating 1-1.5 m during a year, and the error introduced by letting the surface be fixed is negligible compared to the dimension of the aquifer. The flux into the groundwater reservoir is set equal to the difference between precipitation and potential evaporation (250 mm/year, cfr. Table II). The underlaying bedrock boundary is considered as impermeable. At the river side, boundary condition is represented by the mean river stage, 151 m a.m.s.l. (Dirichlet condition) .

By gradually tuning the hydraulic conductivity in each layer we approached the observed hydraulic heads. According to the parameters in Table V the resulting

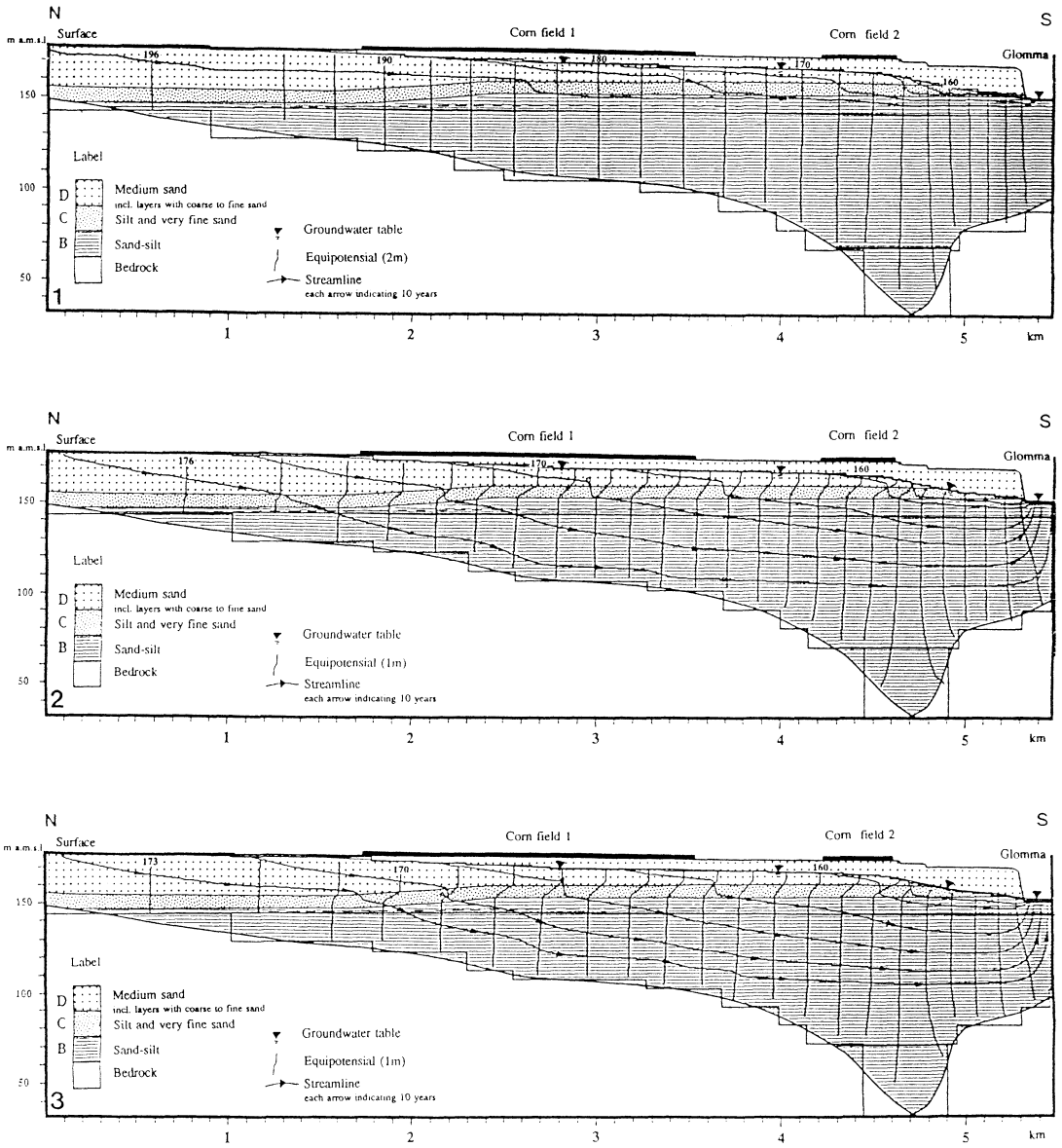

Figure 36. *Three different flow cases with input parameters listed in Table V. The equipotensial lines should correspond to the observed hydraulic heads .*

flow paths are plotted for three different cases in Figure 36. Case 3 is most in accordance with the observed hydraulic heads. In this simplified model we kept porosity and anisotropy constant. A full calibration and validation procedure including a geostatistical analysis will be a topic for further research.

Table V Hydraulic parameters to flow paths in Figure 36. Recharge is assumed 250 mm/year.

Parameters	case 1.	case 2.	case 3.
K_h <m/s> unit D	$1.7 \cdot 10^{-4}$	$1.7 \cdot 10^{-4}$	$1.8 \cdot 10^{-4}$
K_h <m/s> unit C	$2.1 \cdot 10^{-5}$	$3.7 \cdot 10^{-6}$	$3.7 \cdot 10^{-6}$
K_h <m/s> unit B_1	$1.7 \cdot 10^{-4}$	$1.2 \cdot 10^{-4}$	$1.2 \cdot 10^{-4}$
K_h <m/s> unit B_2	$1.1 \cdot 10^{-5}$	$7.6 \cdot 10^{-5}$	$7.6 \cdot 10^{-5}$
K_h <m/s> unit B_3	$1.1 \cdot 10^{-5}$	$3.7 \cdot 10^{-6}$	$3.7 \cdot 10^{-6}$
Effective porosity <%>	20	20	20
Anisotropy, K_h/K_v	4	20	20
Maximum hydraulic head	198	177	173
Residence time from upper field <years>	15-20	25-45	30-50

9 Geochemistry

The content of this chapter is a summary based upon discussions in Englund et al. (1993) and data from Sæland (1987).

The potential pollution of inorganic agricultural fertilizers to the Haslemoen aquifer has been under concern and a subject of study since 1986. A large number of water analyses were given by Sæland (1987), and additional water sampling and analyses have been conducted by the GREGR Haslemoen project through the last 3-4 years. The major part of the Haslemoen area consists of a flat fluvial terrace. Spruce and pine cover the terrace except for a few cultivated fields producing oat and barley. The major crop producing field was deforested in 1952 and fertilized for the first time in 1953. Records of the amount and type of fertilizer applied are available for the whole period up to now, the same is true for the lime supply. Corresponding data are also available for the crop produced, so the annual excess fertilizer available for leaching to the ground water can be estimated. The annual supply has been approximately constant through this period (compare Table VI).

Similarly chemical precipitation data are used to quantify annual atmospheric input to the forested areas.

Table VI Annual areal input of chemical constituents to the Haslemoen area given as kg/da/year estimated for the 1960-1989 period. Forested areas receive only atmospheric precipitation, while input for the fertilized agricultural areas have been estimated for two cases: (A) where only the grain was harvested and (B) where both grain and straw were removed.

	N_{NH4+}	N_{NO3-}	K	Na	Ca	Cl	SO4
Forest	0.6	0.6	0.3	0.6		0.7	3.5
Grain fields(A)	3.9	2.9	6.4		11.3	3.9	11.9
Grain fields(B)	3.3	2.3	2.5		10.4	1.9	11.3

Processes controlling the water chemistry

The background evolution of the ground water chemistry is normally determined by 1) atmospheric precipitation including dry deposition (modified by forrest vegetation interception), 2) uptake/release by the vegetation, 3) soil ion exchange/adsorption and not least 4) mineral weathering and other mineral water reactions. When fertilizers are added in the form of nitrates, phosphates, sulfates and chlorides in addition to other salts, the amounts of dissolved constituents completely mask (compare Table VI) the normal evolutionary trend. However, in unpolluted forested areas and at larger aquifer depth, this background trend is found with a smaller steady increase in Na, K, Ca, Mg, Si and bicarbonate. The same pattern is also reflected in the conductivity measurements from station 23 and the deepest sampling probe at station 48. Waters contaminated by fertilizer exhibit up to 4-6 times more dissolved constituents, and a change of chemical character. Liming in the fertilized areas causes a large increase in bicarbonate, which completely overshadows the amount of bicarbonate produced by silicate mineral weathering. An equivalent amount of Ca + Mg is also dissolved in the soil water. The N and P-fertilizers release a large amount of ammonium, nitrate and sulfate to the soil and ground water. Very little phosphate is washed down to the groundwater as it gets bounded to the upper part of the soil. The surplus ammonium not used by the vegetation is rapidly converted to nitrate by nitrification processes in the soil. Very little ammonium is detected in the ground water, so practically all nitrogen has to be transported as nitrate. Denitrification of nitrate is taking place in the aquifer. This is clearly manifested by the inverse relationship between dissolved organic carbon and nitrate. Oxygen saturation values also correspond to redox conditions where denitrification occurs. However, we have not

been able to express the denitrification quantitatively. An indirect approach will be first to model the spreading of nitrate in the aquifer as a conservative tracer and then to subtract the observed values. The difference constitutes the amount of nitrate lost by denitrification, and from this rough estimates of denitrification rates can be made. Work is planned along those lines.

10 Summary and conclusions

The purpose of developing Haslemoen as a reference field in geohydrology has to some extent been achieved, especially those aspects involving geophysical mapping techniques. The local properties of soil water (very low electrical conductivity) make Haslemoen a well suited area for electrical and electromagnetic methods, e.g. Ground Penetrating Radar (GPR). NGU as well as NGI have tested their equipment during this project. The GPR data from Haslemoen are very promising and constitute one of the most important results from this project.

Some efforts have been made to evaluate pore flow velocities, which is a necessary part in any groundwater flow model dealing with contaminant transport. Valuable experience in handling the practical tests in the field has been gained. Models have been implemented and have increased our understanding of the aquifer. Those models may be applied to similar problems in the future.

To make a synthesis of geology, describing the variability of petrophysical parameters and geochemistry in a 3-D flow model, requires an enormous amount of data, both physical data as core samples, and indirect data as GPR-data. Such a synthesis has not been fully achieved, but further research on the data collected during this project period is planned.

One major aim of this project has been to strengthen the inter-institutional co-operation, in order to improve our ability to solve practical and theoretical problems that we may face in the future as a result of the expected increase of groundwater utilization. This cooperation is established during the Haslemoen-project and will continue in the future.

Acknowledgements

This project - including field work, sampling and data analyses - has been possible to carry out due to the financial support form the Royal Norwegian Council for Scientific and Industrial Research (NTNF) during the "Improved Use of the Water Resources" (BBV) programme. The positive attitude and patience from the NTNF-BBV's staff have promoted the writing of this report.

Each institution involved has supported this work beyond the limits of the financial support; the Norwegian Geotechnical Institute - drilling, georadar and tomography, the Norwegian Geological Survey - georadar, seismics and electrical sounding, Jordforsk - implementation of piezometers, the Norwegian Water Resources and Energy Administration - monitoring and tracer tests, the University of Oslo, Dept. of Geology and Dept. of Geophysics and the Agricultural University of Norway - field work and research, the University of Bergen, Dept. of Geology - tracer test, and last but not least the staff at Haslemoen military base, whose hospitality and practical help during the field work had no bounds.

A big thank to the people at Norwegian Water Resources and Energy Administration who have contributed during this project, especially Øystein Aars who has read through this report.

References

Allen, J. 1992: Regional Groundwater Simulation of an Unconfined Aquifer, Haslemoen, Norway. *Thesis, University of Oslo, Inst. of Geography.*

Bear, J. 1972: Dynamics of Fluids in Porous Media. *American Elsevier, New York*

Bear, J. 1979: Hydraulics of Groundwater. *McGraw-Hill Inc., Israel*

Bear, J. & Verruijt, A. 1987: Modeling Groundwater Flow and Pollution. *D. Reidel Publishing Company, Dordrecht, Holland*

Bjørlykke, K.O. 1901: Om jordbunnen i Solør.*Tidsskr.f.det nor.landbrug 8,604-613.*

Clark, I, 1979: Practical Geostatistics. *Elsevier Applied Science, London, Great Britain*

DNMI,1991: Det Norske MeteorologiskeInstitutt. Meteorological data for weather 1961-1990, Flisa.

Einan, M.B. 1989: En modellering av grunnvannets bevegelse på Haslemoen ved endelige elementers metode. *Thesis, University of Oslo, Inst. of Geography.*

Englund, J.-O.& Haldorsen, S. 1986: Profiles of Nitrogen Species in a Sand-Silt Aquifer at Haslemoen, Solør South Norway. *Nordic Hydrology 17, p295-304*

Englund, J.-O., Hongve, D., & Sæland, S. 1990: Areal use - groundwater quality, particularly with respect to nitrates. Case studies from southeastern Norway. *Norwegian National Institute of Public Health, SIFF VANN rapport nr 78.*

Englund, J.-O., Aagaard, P., Hongve, D. and Hongseth, N.M. (1993). Nitrate transport in an unconfined sandy aquifer: Areal use and ground water chemistry. Haslemoen, Solør, South Norway. (in prep.)

FIDAP, 1991: FIDAP theoretical manual, rev. 6.0. *Fluid Dynamics International, INC, Evanston, Illinois, USA.*

Goffeng, G. Haugen, L.-E. & Løwe, A. 1980: Løsmassekart Flisa, DC061 1:10000. Prøvekart Jordregisterinstituttet. *Norg.geol.unders.*

Goffeng, G. Løwe, A. & Haugen, L.-E. 1981a: Løsmassekart Hovelsåsberget C061 1:10000, Prøvekart Jordregisterinstituttet. *Norg.geol.unders.*

Goffeng, G. Løwe, A. & Haugen, L.-E. 1981b: Løsmassekart Hovelsåsberget & Hollarberget CY061-CY062, 1:20 000, Prøvekart Jordregisterinstituttet. *Norg.geol.unders.*

GREGR 1989: Groundwater Research Group, Annual report 1989. *Norwegian Water Resources and Energy Administration, Oslo.*

Haldorsen, S., Dienboll Jenssen, P. & Samuelsen, J.M. 1986: Hydrogeological properties of the fine sand - coarse silt ('koppjord') in Solør, southeastern Norway. *Nor. geol. tidskr. 66, p223-233*

Hantush M.S. 1961: Drawdown around a partially penetration well.*J. Am. Soc. civ. Engineers, 87, HY4,83-98*

Holmsen, G. 1954: Oppland. Beskrivelse til kvartærgeologsik landgeneralkart. *Norg.geol.unders.187, 58p.*

Høye, T. & Sand, M. 1983: Geofysiske undersøkelser av kvartære sedimenter ved Haslemoen og Flisa, Hedmark. *Thesis, University of Oslo, Inst. of Geology*

Jakobsen, B. 1987: Grunnvannsdannelse, Haslemoen. Et modellstudium.*Thesis, University of Oslo, Inst. of Geophysics.*

Jakobsen, B., Gottschalk, L., Haldorsen, S. & Stensby Høstmark A.K. 1990: Groundwater recharge of fluvial deposits at Haslemoen, Solør, southeastern Norway. *Nor. geol. tidskr. 70, p35-46*

Kinzelbach, W. & Rausch, R. 1989: Aquifer Simulation Model "ASM", Documentation. *Kassel - Universität, FRG*

Kitterød, N.-O. 1991: Fra "Miljøgeologi i praksis", Matematisk modellering av forurensningstransport i grunnvann. Eksempler fra Haslemoen, Solør. *Norsk Sivilingeniørers Forening, Studiesenteret, Kursdagene på NTH, Trondheim. 7-9. januar 1991*

Kong, F.N., By, T.L. & Westerdahl, H. 1990: Underground Radar Imaging Technique in Geotechnical and Environmental Engineering.*First International Seminar on Soil Mechanics and Foundation Engineering of Iran*

Kruseman, G.P. & de Ridder, N.A. 1992: Analysis and Evaluation of Pumping Test Data, Second Edition. *International Institute for Land Reclamation and Improvement, The Netherlands*

Maas, C. 1987: Groundwater Flow to a Well in a Layered Porous Medium 1. Steady Flow. *Water Res. Res., Vol 23, No 8, p1675-1681*

McDonald, M. & Harbaugh, A. 1988: Techniques of Water-Resources Investigations of the United Sates Geological Survey, Book 6. *Scientific Software Group, Washington, D.C., USA*

Morris, M., Rønning, J.S., Kitterød, N.-O., Lile, O.B. 1992: Monotoring of groundwater flow with electrical resistivity at Haslemoen, Hedmark county. *NGU-rapport nr. 92.330. ISSN 0800-3416*

Riis, V. 1992: Hydrogeologi og avsetningsmodell av Haslemoen i Solør.*Thesis, University of Oslo, Inst. of Geology.*

Rønning, J.S. & Kitterød, N.-O. 1992: Ground Penetration Radar at Haslemoen, SE-Norway. *54th E.A.E.G.-meeting in Paris, 1.-5. June 1992. Abstracts of papers p656-657.*

Rønning, J.S. & Mauring, E. 1991: Georadar og refleksjonsseismiske målinger på Haslemoen.*NGU-rapport nr. 91.270, ISSN 0800-3416*

Sortdal, K.K. 1921: Jordbunden i Solødalføret. Det kgl. Selsk. for Norges Vels jordbundsutvalg. *Jordbundsbedkrivelse 18, 39p.*

Székely, F. 1992: Pumping test data analysis in wells with multiple or long screens. *Journal of Hydrology, 132,p137-156*

Sudicky, E.A. 1986: A Natural Gradient Experiment on Solute Transport in a Sand Aquifer: SpatialVariability of Hydraulic Conductivity and Its Role in the Dispersion Process. *Water Res. Res. Vol. 22, No13, p2069-2082*

Sæland, S. (1987). Arealbruk - Nitratbelasting på grunnvatn. *Thesis, Norwegian Agricultural University, Ås*

Veling, E.J.M 1991: FLOP3N - Pathlines in Three-Dimensional Groundwater Flow in a System of Homogeneous Anisotropic Layers, Report no. 719106001. *National Institute of Public Health and Environmental Protection, Bilthoven, The Netherlands.*

Wikramaratna, R.S. 1984: An Analytical Solution for the Effects of Abstraction From a Multiple-Layerd Confined Aquifer With No Cross Flow. *Water Res. Res. Vol.20, p1067-1074.*

Appendix

Tabel <A>. Subfunction W(u), u=(r²S)/(4tkD). Cfr. f.ex. Bear, 1979, table 8-2, p.320

u	W(u)	u	W(u)	u	W(u)	u	W(u)
.10 E+01	.2193913	.10 E-03	8.6332404	.10 E-07	17.8434808	.10 E-11	27.0538211
.15 E+01	.1000015	.15 E-03	8.2278253	.15 E-07	17.4380157	.15 E-11	26.6483560
.20 E+01	.0507238	.20 E-03	7.9401932	.20 E-07	17.1503336	.20 E-11	26.3606739
.25 E+01	.0257287	.25 E-03	7.7170996	.25 E-07	16.9271900	.25 E-11	26.1375304
.30 E+01	.0130504	.30 E-03	7.5348281	.30 E-07	16.7448685	.30 E-11	25.9552088
.35 E+01	.0069714	.35 E-03	7.3807274	.35 E-07	16.5907178	.35 E-11	25.8010582
.40 E+01	.0038215	.40 E-03	7.2472460	.40 E-07	16.4571864	.40 E-11	25.6675268
.45 E+01	.0020948	.45 E-03	7.1295129	.45 E-07	16.3394034	.45 E-11	25.5497437
.50 E+01	.0011483	.50 E-03	7.0242024	.50 E-07	16.2340429	.50 E-11	25.4443832
.55 E+01	.0006409	.55 E-03	6.9289422	.55 E-07	16.1387327	.55 E-11	25.3490730
.60 E+01	.0003651	.60 E-03	6.8419808	.60 E-07	16.0517213	.60 E-11	25.2620617
.65 E+01	.0002079	.65 E-03	6.7619881	.65 E-07	15.9716786	.65 E-11	25.1820189
.70 E+01	.0001184	.70 E-03	6.6879301	.70 E-07	15.8975707	.70 E-11	25.1079110
.75 E+01	.0000675	.75 E-03	6.6189872	.75 E-07	15.8285778	.75 E-11	25.0389181
.80 E+01	.0000384	.80 E-03	6.5544987	.80 E-07	15.7640393	.80 E-11	24.9743796
.85 E+01	.0000219	.85 E-03	6.4939240	.85 E-07	15.7034147	.85 E-11	24.9137550
.90 E+01	.0000125	.90 E-03	6.4368156	.90 E-07	15.6462563	.90 E-11	24.8565965
.95 E+01	.0000071	.95 E-03	6.3827984	.95 E-07	15.5921890	.95 E-11	24.8025293
.10 E+00	1.8229396	.10 E-04	10.9357355	.10 E-08	20.1460658	.10 E-12	29.3564062
.15 E+00	1.4644773	.15 E-04	10.5302754	.15 E-08	19.7406007	.15 E-12	28.9509411
.20 E+00	1.2226662	.20 E-04	10.2425983	.20 E-08	19.4529187	.20 E-12	28.6632590
.25 E+00	1.0442983	.25 E-04	10.0194597	.25 E-08	19.2297751	.25 E-12	28.4401155
.30 E+00	.9056923	.30 E-04	9.8371432	.30 E-08	19.0474536	.30 E-12	28.2577939
.35 E+00	.7942311	.35 E-04	9.6829975	.35 E-08	18.8933029	.35 E-12	28.1036432
.40 E+00	.7023958	.40 E-04	9.5494711	.40 E-08	18.7597715	.40 E-12	27.9701119
.45 E+00	.6253470	.45 E-04	9.4316931	.45 E-08	18.6419884	.45 E-12	27.8523288
.50 E+00	.5597893	.50 E-04	9.3263376	.50 E-08	18.5366279	.50 E-12	27.7469683
.55 E+00	.5033797	.55 E-04	9.2310324	.55 E-08	18.4413178	.55 E-12	27.6516581
.60 E+00	.4543952	.60 E-04	9.1440260	.60 E-08	18.3543064	.60 E-12	27.5646467
.65 E+00	.4115326	.65 E-04	9.0639883	.65 E-08	18.2742637	.65 E-12	27.4846040
.70 E+00	.3737845	.70 E-04	8.9898853	.70 E-08	18.2001557	.70 E-12	27.4104961
.75 E+00	.3403564	.75 E-04	8.9208974	.75 E-08	18.1311628	.75 E-12	27.3415032
.80 E+00	.3106120	.80 E-04	8.8563639	.80 E-08	18.0666243	.80 E-12	27.2769647
.85 E+00	.2840342	.85 E-04	8.7957443	.85 E-08	18.0059997	.85 E-12	27.2163400
.90 E+00	.2601979	.90 E-04	8.7385909	.90 E-08	17.9488413	.90 E-12	27.1591816
.95 E+00	.2387494	.95 E-04	8.6845287	.95 E-08	17.8947741	.95 E-12	27.1051144
.10 E-01	4.0379452	.10 E-05	13.2383116	.90 E-09	20.2514264	.10 E-13	31.6589913
.95 E-01	1.8694689	.15 E-05	12.8328470	.10 E-09	22.4486509	.15 E-13	31.2535262
.15 E-01	3.6374490	.20 E-05	12.5451654	.15 E-09	22.0431858	.20 E-13	30.9658441
.20 E-01	3.3547235	.25 E-05	12.3220223	.20 E-09	21.7555038	.25 E-13	30.7427006
.25 E-01	3.1365241	.30 E-05	12.1397013	.25 E-09	21.5323602	.30 E-13	30.5603790
.30 E-01	2.9591344	.35 E-05	11.9855511	.30 E-09	21.3500386	.35 E-13	30.4062283
.35 E-01	2.8099033	.40 E-05	11.8520202	.35 E-09	21.1958880	.40 E-13	30.2726969
.40 E-01	2.6812794	.45 E-05	11.7342377	.40 E-09	21.0623566	.45 E-13	30.1549139
.45 E-01	2.5683916	.50 E-05	11.6288777	.45 E-09	20.9445735	.50 E-13	30.0495534
.50 E-01	2.4679142	.55 E-05	11.5335680	.50 E-09	20.8392130	.55 E-13	29.9542432
.55 E-01	2.3774750	.60 E-05	11.4465571	.55 E-09	20.7439028	.60 E-13	29.8672318
.60 E-01	2.2953226	.65 E-05	11.3665149	.60 E-09	20.6568915	.65 E-13	29.7871891
.65 E-01	2.2201268	.70 E-05	11.2924074	.65 E-09	20.5768488	.70 E-13	29.7130812
.70 E-01	2.1508538	.75 E-05	11.2234150	.70 E-09	20.5027408	.75 E-13	29.6440883
.75 E-01	2.0866840	.80 E-05	11.1588770	.75 E-09	20.4337479	.80 E-13	29.5795498
.80 E-01	2.0269567	.85 E-05	11.0982529	.80 E-09	20.3692094	.85 E-13	29.5189251
.85 E-01	1.9711314	.90 E-05	11.0410950	.85 E-09	20.3085848	.90 E-13	29.4617667
.90 E-01	1.9187604	.95 E-05	10.9870283	.95 E-09	20.1973591	.95 E-13	29.4076995
.10 E-02	6.3315550	.10 E-06	15.5408958	.10 E-10	24.7512360	.10 E-14	33.9615764
.15 E-02	5.9265896	.15 E-06	15.1354307	.15 E-10	24.3457709	.15 E-14	33.5561113
.20 E-02	5.6394071	.20 E-06	14.8477487	.20 E-10	24.0580888	.20 E-14	33.2684292
.25 E-02	5.4167630	.25 E-06	14.6246052	.25 E-10	23.8349453	.25 E-14	33.0452857
.30 E-02	5.2349407	.30 E-06	14.4422837	.30 E-10	23.6526237	.30 E-14	32.8629641
.35 E-02	5.0812893	.35 E-06	14.2881330	.35 E-10	23.4984731	.35 E-14	32.7088134
.40 E-02	4.9482569	.40 E-06	14.1546017	.40 E-10	23.3649417	.40 E-14	32.5752820
.45 E-02	4.8309728	.45 E-06	14.0368187	.45 E-10	23.2471586	.45 E-14	32.4574990
.50 E-02	4.7261111	.50 E-06	13.9314582	.50 E-10	23.1417981	.50 E-14	32.3521385
.55 E-02	4.6312996	.55 E-06	13.8361481	.55 E-10	23.0464879	.55 E-14	32.2568283
.60 E-02	4.5447868	.60 E-06	13.7491368	.60 E-10	22.9594766	.60 E-14	32.1698169
.65 E-02	4.4652426	.65 E-06	13.6690941	.65 E-10	22.8794339	.65 E-14	32.0897742
.70 E-02	4.3916329	.70 E-06	13.5949862	.70 E-10	22.8053259	.70 E-14	32.0156663
.75 E-02	4.3231382	.75 E-06	13.5259934	.75 E-10	22.7363330	.75 E-14	31.9466734
.80 E-02	4.2590978	.80 E-06	13.4614549	.80 E-10	22.6717945	.80 E-14	31.8821349
.85 E-02	4.1989711	.85 E-06	13.4008303	.85 E-10	22.6111699	.85 E-14	31.8215102
.90 E-02	4.1423105	.90 E-06	13.3436720	.90 E-10	22.5540115	.90 E-14	31.7643518
.95 E-02	4.0887410	.95 E-06	13.2896048	.95 E-10	22.4999442	.95 E-14	31.7102846

Table <B> Results form SUBFUNCTIONS FSB.FOR and FSA.FOR, $\beta=r/D*(k_z/k_h)^{1/2}$ (cfr. Krauseman and de Ridder, 1991 Annex 8.1 p314, tab.8.1)

Values of f for b/D = 1.0 and d/D = 0.9

β	z/D=0.1	z/D=0.4	z/D=1.0
.05	-4.784	-4.018	21.226
.10	-3.416	-2.673	11.402
.15	-2.633	-1.925	7.086
.20	-2.095	-1.433	4.777
.25	-1.696	-1.086	3.393
.30	-1.387	-.833	2.498
.35	-1.142	-.645	1.887
.40	-.944	-.503	1.454
.45	-.783	-.395	1.136
.50	-.650	-.312	.899
.55	-.541	-.248	.718
.60	-.451	-.198	.578
.65	-.376	-.159	.468
.70	-.314	-.128	.381
.75	-.262	-.104	.312
.80	-.219	-.085	.256
.85	-.183	-.069	.211
.90	-.154	-.057	.174
.95	-.129	-.047	.144
1.00	-.108	-.039	.120
1.05	-.090	-.032	.099
1.10	-.076	-.026	.083
1.15	-.064	-.022	.069
1.20	-.053	-.018	.058
1.25	-.045	-.015	.048
1.30	-.038	-.013	.040
1.35	-.032	-.011	.034
1.40	-.027	-.009	.028
1.45	-.022	-.007	.024
1.50	-.019	-.006	.020
1.55	-.016	-.005	.017
1.60	-.013	-.004	.014
1.65	-.011	-.004	.012

Values of f_m for b/D = 1.0 and d/D = 0.9

β	do=0.9 bo=1.1	do=0.9 bo=3.1	do=0.9 bo=7.1
.05	-4.784	-4.629	-3.617
.10	-3.416	-3.264	-2.303
.15	-2.633	-2.487	-1.602
.20	-2.095	-1.957	-1.160
.25	-1.696	-1.567	-.862
.30	-1.387	-1.269	-.653
.35	-1.142	-1.034	-.502
.40	-.944	-.847	-.390
.45	-.782	-.696	-.307
.50	-.650	-.574	-.243
.55	-.541	-.475	-.194
.60	-.451	-.393	-.156
.65	-.376	-.326	-.126
.70	-.314	-.271	-.102
.75	-.262	-.225	-.084
.80	-.219	-.187	-.069
.85	-.183	-.156	-.056
.90	-.153	-.130	-.046
.95	-.129	-.109	-.038
1.00	-.108	-.091	-.032
1.05	-.090	-.076	-.026
1.10	-.076	-.064	-.022
1.15	-.064	-.053	-.018
1.20	-.053	-.045	-.015
1.25	-.045	-.038	-.013
1.30	-.038	-.032	-.011
1.35	-.032	-.027	-.009
1.40	-.027	-.022	-.007
1.45	-.022	-.019	-.006
1.50	-.019	-.016	-.005
1.55	-.016	-.013	-.004
1.60	-.013	-.011	-.004
1.65	-.011	-.009	-.003

Table <C> Modified Bessel-function of second kind, order zero. (Cfr. Bear, 1979, Table 8-1 p 4)

x	Ko(x)	x	Ko(x)
.010	4.72124	.550	.84657
.015	4.31594	.600	.77752
.020	4.02846	.650	.71587
.025	3.80556	.700	.66052
.030	3.62353	.750	.61058
.035	3.46971	.800	.56535
.040	3.33654	.850	.52423
.045	3.21916	.900	.48673
.050	3.11423	.950	.45245
.055	3.01939	1.000	.42102
.060	2.93288	1.500	.21381
.065	2.85337	2.000	.11389
.070	2.77982	2.500	.06235
.075	2.71141	3.000	.03474
.080	2.64749	3.500	.01960
.085	2.58751	4.000	.01116
.090	2.53102	4.500	.00640
.095	2.47764	5.000	.00369
.100	2.42707	5.500	.00214
.150	2.03003	6.000	.00124
.200	1.75270	6.500	.00073
.250	1.54151	7.000	.00042
.300	1.37246	7.500	.00025
.350	1.23271	8.000	.00015
.400	1.11453	8.500	.00009
.450	1.01291	9.000	.00005
.500	.92442	9.500	.00003

Denne serien utgis av Norges vassdrags- og energiverk (NVE)
Adresse: Postboks 5091 Majorstua, 0301 Oslo

I 1994 ER FØLGENDE RAPPORTER UTGITT:

Nr 1 Truls Erik Bønsnes og Lars Andreas Roald: Regional flomfrekvensanalyse. Sambandet mellom momentanflom og døgnmiddelflom. (45 s.)

Nr 2 Steinar Myrabø: Sæternbekken forsøksfelt. (29 s.)

Nr 3 Edward Witczak: Vurdering av grustak i Stjørdalselva ved Måsøra - Hofstadøra. Stjørdal kommune, N-Trøndelag. Vassdrag nr. 124. A0. (11 s.)

Nr 4 Bjarne Krokli: Q 100 og Q 1000 avløpsflom med naturlig utløpsprofil i Ulldalsvatn og Bergsvatn (079.Z). (13 s.)

Nr 5 Rune Dahl, Hans Otnes og Frode Trengereid: Årsrapport for NVEs interne havarigruppe. (8 s.)

Nr 6 Harald Sakshaug: Vassdragsteknisk vurdering av interimsvei ved bygging av ny Vikersund bru. (5 s.)

Nr 7 Astrid Voksø, Bjarne Krokli: Flomlinjeberegning og flomsonekart for nedre del av Leira (002. CAZ). (9 s.)

Nr 8 Lars-Evan Pettersson: Flomberegning Lærdalsvassdraget (073.Z). (36 s.)

Nr 9 Ole Einar Tveito og Hege Hisdal: A study of regional trends in annual and seasonal precipitation and runoff series. (30 s.)

Nr 10 Einar Beheim, Eirik Smidt Eriksen: Vassdragsteknisk seksjon 1993. (73 s.)

Nr 11 Nils-Otto Kitterød: The Haslemoen-project - main results and experiences. (56s.)